



HAL
open science

Search for pair-produced neutralinos in events with photons and missing energy from e^+e^- collisions at $\sqrt{s} = 130-183$ GeV

P. Abreu, T. Adye, P. Adzic, I. Ajinenko, G D. Alekseev, R. Alemany, P P. Allport, S. Almeded, U. Amaldi, S. Amato, et al.

► To cite this version:

P. Abreu, T. Adye, P. Adzic, I. Ajinenko, G D. Alekseev, et al.. Search for pair-produced neutralinos in events with photons and missing energy from e^+e^- collisions at $\sqrt{s} = 130-183$ GeV. European Physical Journal C: Particles and Fields, 1999, 6, pp.371-384. 10.1007/s100529801044 . in2p3-00001125

HAL Id: in2p3-00001125

<https://in2p3.hal.science/in2p3-00001125v1>

Submitted on 19 Jan 1999

HAL is a multi-disciplinary open access archive for the deposit and dissemination of scientific research documents, whether they are published or not. The documents may come from teaching and research institutions in France or abroad, or from public or private research centers.

L'archive ouverte pluridisciplinaire **HAL**, est destinée au dépôt et à la diffusion de documents scientifiques de niveau recherche, publiés ou non, émanant des établissements d'enseignement et de recherche français ou étrangers, des laboratoires publics ou privés.

Search for pair-produced neutralinos in events with photons and missing energy from e^+e^- collisions at $\sqrt{s}=130-183$ GeV

DELPHI Collaboration

Abstract

The events with two photons and missing (transverse) energy collected by the DELPHI detector at centre-of-mass energies between 130 GeV and 183 GeV have been studied to search for processes of the type $e^+e^- \rightarrow YY$ with the subsequent decay $Y \rightarrow X\gamma$, where X is an undetectable neutral particle. Reactions of this kind are expected in supersymmetric models, where the Y particle can be either the lightest neutralino, decaying to a photon and a gravitino, or the next-to-lightest neutralino, decaying to a photon and the lightest neutralino. To study the case of long-lived Y particles, a search for single-photon events with the reconstructed photon axis pointing far from the beam interaction region has also been performed. No evidence for a deviation from Standard Model expectations has been observed in the data and upper limits have been derived on the signal cross-section as a function of the the X and Y masses and of the Y mean decay path.

(Accepted by E. Phys. J. C)

P.Abreu²¹, T.Adye³⁶, P.Adzic¹¹, I.Ajinenko⁴², G.D.Alekseev¹⁶, R.Aleman⁴⁹, P.P.Allport²², S.Almehed²⁴, U.Amaldi⁹, S.Amato⁴⁷, E.G.Anassontzis³, P.Andersson⁴⁴, A.Andreazza⁹, S.Andringa²¹, P.Antilogus²⁵, W-D.Apel¹⁷, Y.Arnaud¹⁴, B.Äsman⁴⁴, J-E.Augustin²⁵, A.Augustinus⁹, P.Baillon⁹, P.Bambade¹⁹, F.Barao²¹, G.Barbiellini⁴⁶, R.Barbier²⁵, D.Y.Bardin¹⁶, G.Barker⁹, A.Baroncelli³⁸, M.Battaglia¹⁵, M.Baubillier²³, K-H.Becks⁵², M.Begalli⁶, P.Beilliere⁸, Yu.Belokopytov^{9,53}, A.C.Benvenuti⁵, C.Berat¹⁴, M.Berggren²⁵, D.Bertini²⁵, D.Bertrand², M.Besancon³⁹, F.Bianchi⁴⁵, M.Bigi⁴⁵, M.S.Bilenky¹⁶, M-A.Bizouard¹⁹, D.Bloch¹⁰, H.M.Blom³⁰, M.Bonesini²⁷, W.Bonivento²⁷, M.Boonekamp³⁹, P.S.L.Booth²², A.W.Borgland⁴, G.Borisov¹⁹, C.Bosio⁴¹, O.Botner⁴⁸, E.Boudinov³⁰, B.Bouquet¹⁹, C.Bourdarios¹⁹, T.J.V.Bowcock²², I.Boyko¹⁶, I.Bozovic¹¹, M.Bozzo¹³, P.Branchini³⁸, T.Brenke⁵², R.A.Brenner⁴⁸, P.Bruckman¹⁸, J-M.Brunet⁸, L.Bugge³², T.Buran³², T.Burgsmueller⁵², P.Buschmann⁵², S.Cabrera⁴⁹, M.Caccia²⁷, M.Calvi²⁷, A.J.Camacho Rozas⁴⁰, T.Camporesi⁹, V.Canale³⁷, F.Carena⁹, L.Carroll²², C.Caso¹³, M.V.Castillo Gimenez⁴⁹, A.Cattai⁹, F.R.Cavallo⁵, Ch.Cerruti¹⁰, V.Chabaud⁹, Ph.Charpentier⁹, L.Chaussard²⁵, P.Checchia³⁵, G.A.Chelkov¹⁶, R.Chierici⁴⁵, P.Chliapnikov⁴², P.Chochula⁷, V.Chorowicz²⁵, J.Chudoba²⁹, P.Collins⁹, M.Colomer⁴⁹, R.Contri¹³, E.Cortina⁴⁹, G.Cosme¹⁹, F.Cossutti³⁹, J-H.Cowell²², H.B.Crawley¹, D.Crennell³⁶, G.Crosetti¹³, J.Cuevas Maestro³³, S.Czellar¹⁵, G.Damgaard²⁸, M.Davenport⁹, W.Da Silva²³, A.Deghorain², G.Della Ricca⁴⁶, P.Delpierre²⁶, N.Demaria⁹, A.De Angelis⁹, W.De Boer¹⁷, S.De Brabandere², C.De Clercq², B.De Lotto⁴⁶, A.De Min³⁵, L.De Paula⁴⁷, H.Dijkstra⁹, L.Di Ciaccio³⁷, A.Di Diodato³⁷, J.Dolbeau⁸, K.Doroba⁵¹, M.Dracos¹⁰, J.Drees⁵², M.Dris³¹, A.Duperrin²⁵, J-D.Durand^{25,9}, R.Ehret¹⁷, G.Eigen⁴, T.Ekelof⁴⁸, G.Ekspong⁴⁴, M.Ellert⁴⁸, M.Elsing⁹, J-P.Engel¹⁰, B.Erzen⁴³, M.Espirito Santo²¹, E.Falk²⁴, G.Fanourakis¹¹, D.Fassouliotis¹¹, J.Fayot²³, M.Feindt¹⁷, P.Ferrari²⁷, A.Ferrer⁴⁹, E.Ferrer-Ribas¹⁹, S.Fichet²³, A.Firestone¹, P.-A.Fischer⁹, U.Flagmeyer⁵², H.Foeth⁹, E.Fokitis³¹, F.Fontanelli¹³, B.Franek³⁶, A.G.Frodesen⁴, R.Fruhvirth⁵⁰, F.Fulda-Quenzer¹⁹, J.Fuster⁴⁹, A.Galloni²², D.Gamba⁴⁵, S.Gamblin¹⁹, M.Gandelman⁴⁷, C.Garcia⁴⁹, J.Garcia⁴⁰, C.Gaspar⁹, M.Gaspar⁴⁷, U.Gasparini³⁵, Ph.Gavillet⁹, E.N.Gazis³¹, D.Gele¹⁰, J-P.Gerber¹⁰, L.Gerdyukov⁴², N.Ghodbane²⁵, I.Gil⁴⁹, F.Glege⁵², R.Gokieli⁵¹, B.Golob⁴³, P.Goncalves²¹, I.Gonzalez Caballero⁴⁰, G.Gopal³⁶, L.Gorn^{1,54}, M.Gorski⁵¹, Yu.Gouz⁴², V.Gracco¹³, J.Grahl¹, E.Graziani³⁸, C.Green²², P.Gris³⁹, K.Grzelak⁵¹, M.Gunther⁴⁸, J.Guy³⁶, F.Hahn⁹, S.Hahn⁵², S.Haider⁹, A.Hallgren⁴⁸, K.Hamacher⁵², F.J.Harris³⁴, V.Hedberg²⁴, S.Heising¹⁷, J.J.Hernandez⁴⁹, P.Herquet², H.Herr⁹, T.L.Hessing³⁴, J.-M.Heuser⁵², E.Higon⁴⁹, S-O.Holmgren⁴⁴, P.J.Holt³⁴, D.Holthuizen³⁰, S.Hoorelbeke², M.Houlden²², J.Hrubic⁵⁰, K.Huet², K.Hultqvist⁴⁴, J.N.Jackson²², R.Jacobsson⁹, P.Jalocha⁹, R.Janik⁷, Ch.Jarlskog²⁴, G.Jarlskog²⁴, P.Jarry³⁹, B.Jean-Marie¹⁹, E.K.Johansson⁴⁴, P.Jonsson²⁴, C.Joram⁹, P.Juillot¹⁰, F.Kapusta²³, K.Karafasoulis¹¹, S.Katsanevas²⁵, E.C.Katsoufis³¹, R.Keranen¹⁷, B.A.Khomenko¹⁶, N.N.Khovanski¹⁶, A.Kiiskinen¹⁵, B.King²², N.J.Kjaer³⁰, O.Klapp⁵², H.Klein⁹, P.Kluit³⁰, D.Knoblauch¹⁷, P.Kokkinias¹¹, M.Koratzinos⁹, V.Kostioukhine⁴², C.Kourkoumelis³, O.Kouznetsov¹⁶, M.Krammer⁵⁰, C.Kreuter⁹, E.Kriznic⁴³, J.Krstic¹¹, Z.Krumstein¹⁶, P.Kubinec⁷, W.Kucewicz¹⁸, K.Kurvinen¹⁵, J.W.Lamsa¹, D.W.Lane¹, P.Langefeld⁵², V.Lapin⁴², J-P.Laugier³⁹, R.Lauhakangas¹⁵, G.Leder⁵⁰, F.Ledroit¹⁴, V.Lefebure², L.Leinonen⁴⁴, A.Leisos¹¹, R.Leitner²⁹, J.Lemonne², G.Lenzen⁵², V.Lepeltier¹⁹, T.Lesiak¹⁸, M.Lethuillier³⁹, J.Libby³⁴, D.Liko⁹, A.Lipniacka⁴⁴, I.Lippi³⁵, B.Loerstad²⁴, J.G.Loken³⁴, J.H.Lopes⁴⁷, J.M.Lopez⁴⁰, R.Lopez-Fernandez¹⁴, D.Loukas¹¹, P.Lutz³⁹, L.Lyons³⁴, J.MacNaughton⁵⁰, J.R.Mahon⁶, A.Maio²¹, A.Malek⁵², T.G.M.Malmgren⁴⁴, V.Malychev¹⁶, F.Mandl⁵⁰, J.Marco⁴⁰, R.Marco⁴⁰, B.Marechal⁴⁷, M.Margoni³⁵, J-C.Marin⁹, C.Mariotti⁹, A.Markou¹¹, C.Martinez-Rivero¹⁹, F.Martinez-Vidal⁴⁹, S.Marti i Garcia²², N.Mastroiannopoulos¹¹, F.Matorras⁴⁰, C.Matteuzzi²⁷, G.Matthiae³⁷, J.Mazik²⁹, F.Mazzucato³⁵, M.Mazzucato³⁵, M.Mc Cubbin²², R.Mc Kay¹, R.Mc Nulty⁹, G.Mc Pherson²², C.Meroni²⁷, W.T.Meyer¹, A.Miagkov⁴², E.Migliore⁴⁵, L.Mirabito²⁵, W.A.Mitaroff⁵⁰, U.Mjoernmark²⁴, T.Moa⁴⁴, R.Moeller²⁸, K.Moenig⁹, M.R.Monge¹³, X.Moreau²³, P.Morettini¹³, G.Morton³⁴, U.Mueller⁵², K.Muenich⁵², M.Mulders³⁰, C.Mulet-Marquis¹⁴, R.Muresan²⁴, W.J.Murray³⁶, B.Muryn^{14,18}, G.Myatt³⁴, T.Myklebust³², F.Naraghi¹⁴, F.L.Navarria⁵, S.Navas⁴⁹, K.Nawrocki⁵¹, P.Negri²⁷, N.Neufeld⁹, N.Neumeister⁵⁰, R.Nicolaidou¹⁴, B.S.Nielsen²⁸, V.Nikolaenko¹⁰, M.Nikolenko^{10,16}, V.Nomokonov¹⁵, A.Normand²², A.Nygren²⁴, V.Obraztsov⁴², A.G.Olshevski¹⁶, A.Onofre²¹, R.Orava¹⁵, G.Orazi¹⁰, K.Osterberg¹⁵, A.Ouraou³⁹, M.Paganoni²⁷, S.Paiano⁵, R.Pain²³, R.Paiva²¹, J.Palacios³⁴, H.Palka¹⁸, Th.D.Papadopoulou³¹, K.Papageorgiou¹¹, L.Pape⁹, C.Parkes³⁴, F.Parodi¹³, U.Parzefall²², A.Passeri³⁸, O.Passon⁵², M.Pegoraro³⁵, L.Peralta²¹, M.Pernicka⁵⁰, A.Perrotta⁵, C.Petridou⁴⁶, A.Petrolini¹³, H.T.Phillips³⁶, G.Piana¹³, F.Pierre³⁹, M.Pimenta²¹, E.Piotto²⁷, T.Podobnik⁴³, M.E.Pol⁶, G.Polok¹⁸, P.Poropat⁴⁶, V.Pozdniakov¹⁶, P.Privitera³⁷, N.Pukhaeva¹⁶, A.Pullia²⁷, D.Radojicic³⁴, S.Ragazzi²⁷, H.Rahmani³¹, D.Rakoczy⁵⁰, P.N.Ratoff²⁰, A.L.Read³², P.Rebecchi⁹, N.G.Redaeli²⁷, M.Regler⁵⁰, D.Reid⁹, R.Reinhardt⁵², P.B.Renton³⁴, L.K.Resvanis³, F.Richard¹⁹, J.Ridky¹², G.Rinaudo⁴⁵, O.Rohne³², A.Romero⁴⁵, P.Ronchese³⁵, E.I.Rosenberg¹, P.Rosinsky⁷, P.Roudeau¹⁹, T.Rovelli⁵, V.Ruhlmann-Kleider³⁹, A.Ruiz⁴⁰, H.Saarikko¹⁵, Y.Sacquin³⁹, A.Sadovsky¹⁶, G.Sajot¹⁴, J.Salt⁴⁹, D.Sampsonidis¹¹, M.Sannino¹³, H.Schneider¹⁷, Ph.Schwemling²³, U.Schwickerath¹⁷, M.A.E.Schyns⁵², F.Scuri⁴⁶, P.Seager²⁰, Y.Sedykh¹⁶, A.M.Segar³⁴, R.Sekulin³⁶, R.C.Shellard⁶, A.Sheridan²², M.Siebel⁵², R.Silvestre³⁹, L.Simard³⁹, F.Simonetto³⁵, A.N.Sisakian¹⁶, T.B.Skaali³², G.Smadja²⁵, O.Smirnova²⁴, G.R.Smith³⁶, A.Sokolov⁴², A.Sopczak¹⁷, R.Sosnowski⁵¹, T.Spaso²¹, E.Spiriti³⁸, P.Sponholz⁵², S.Squarcia¹³, D.Stamper⁵⁰, C.Stanescu³⁸, S.Stanic⁴³, S.Stapnes³², K.Stevenson³⁴, A.Stocchi¹⁹, J.Strauss⁵⁰, R.Strub¹⁰, B.Stugu⁴, M.Szczekowski⁵¹, M.Szeptycka⁵¹, T.Tabarelli²⁷, O.Tchikilev⁴², F.Tegenfeldt⁴⁸, F.Terranova²⁷, J.Thomas³⁴, A.Tilquin²⁶, J.Timmermans³⁰, L.G.Tkatchev¹⁶, T.Todorov¹⁰, S.Todorova¹⁰, D.Z.Toet³⁰, A.Tomaradze², B.Tome²¹, A.Tonazzo²⁷, L.Tortora³⁸,

G. Transtrome²⁴, D. Treille⁹, G. Tristram⁸, C. Troncon²⁷, A. Tsirou⁹, M.-L. Turluer³⁹, I.A. Tyapkin¹⁶, S. Tzamarias¹¹, B. Ueberschaer⁵², O. Ullaland⁹, V. Uvarov⁴², G. Valenti⁵, E. Vallazza⁴⁶, G.W. Van Apeldoorn³⁰, P. Van Dam³⁰, W.K. Van Doninck², J. Van Eldik³⁰, A. Van Lysebetten², I. Van Vulpen³⁰, N. Vassilopoulos³⁴, G. Vegni²⁷, L. Ventura³⁵, W. Venus³⁶, F. Verbeure², M. Verlato³⁵, L.S. Vertogradov¹⁶, V. Verzi³⁷, D. Vilanova³⁹, L. Vitale⁴⁶, E. Vlasov⁴², A.S. Vodopyanov¹⁶, G. Voulgaris³, V. Vrba¹², H. Wahlen⁵², C. Walck⁴⁴, C. Weiser¹⁷, D. Wicke⁵², J.H. Wickens², G.R. Wilkinson⁹, M. Winter¹⁰, M. Witek¹⁸, G. Wolf⁹, J. Yi¹, O. Yushchenko⁴², A. Zalewska¹⁸, P. Zalewski⁵¹, D. Zavrtnik⁴³, E. Zevgolatakos¹¹, N.I. Zimin^{16,24}, G.C. Zucchelli⁴⁴, G. Zumerle³⁵

¹Department of Physics and Astronomy, Iowa State University, Ames IA 50011-3160, USA

²Physics Department, Univ. Instelling Antwerpen, Universiteitsplein 1, BE-2610 Wilrijk, Belgium and IIHE, ULB-VUB, Pleinlaan 2, BE-1050 Brussels, Belgium

and Faculté des Sciences, Univ. de l'Etat Mons, Av. Maistriau 19, BE-7000 Mons, Belgium

³Physics Laboratory, University of Athens, Solonos Str. 104, GR-10680 Athens, Greece

⁴Department of Physics, University of Bergen, Allégaten 55, NO-5007 Bergen, Norway

⁵Dipartimento di Fisica, Università di Bologna and INFN, Via Irnerio 46, IT-40126 Bologna, Italy

⁶Centro Brasileiro de Pesquisas Físicas, rua Xavier Sigaud 150, BR-22290 Rio de Janeiro, Brazil

and Depto. de Física, Pont. Univ. Católica, C.P. 38071 BR-22453 Rio de Janeiro, Brazil

and Inst. de Física, Univ. Estadual do Rio de Janeiro, rua São Francisco Xavier 524, Rio de Janeiro, Brazil

⁷Comenius University, Faculty of Mathematics and Physics, Mlynska Dolina, SK-84215 Bratislava, Slovakia

⁸Collège de France, Lab. de Physique Corpusculaire, IN2P3-CNRS, FR-75231 Paris Cedex 05, France

⁹CERN, CH-1211 Geneva 23, Switzerland

¹⁰Institut de Recherches Subatomiques, IN2P3 - CNRS/ULP - BP20, FR-67037 Strasbourg Cedex, France

¹¹Institute of Nuclear Physics, N.C.S.R. Demokritos, P.O. Box 60228, GR-15310 Athens, Greece

¹²FZU, Inst. of Phys. of the C.A.S. High Energy Physics Division, Na Slovance 2, CZ-180 40, Praha 8, Czech Republic

¹³Dipartimento di Fisica, Università di Genova and INFN, Via Dodecaneso 33, IT-16146 Genova, Italy

¹⁴Institut des Sciences Nucléaires, IN2P3-CNRS, Université de Grenoble 1, FR-38026 Grenoble Cedex, France

¹⁵Helsinki Institute of Physics, HIP, P.O. Box 9, FI-00014 Helsinki, Finland

¹⁶Joint Institute for Nuclear Research, Dubna, Head Post Office, P.O. Box 79, RU-101 000 Moscow, Russian Federation

¹⁷Institut für Experimentelle Kernphysik, Universität Karlsruhe, Postfach 6980, DE-76128 Karlsruhe, Germany

¹⁸Institute of Nuclear Physics and University of Mining and Metallurgy, Ul. Kawory 26a, PL-30055 Krakow, Poland

¹⁹Université de Paris-Sud, Lab. de l'Accélérateur Linéaire, IN2P3-CNRS, Bât. 200, FR-91405 Orsay Cedex, France

²⁰School of Physics and Chemistry, University of Lancaster, Lancaster LA1 4YB, UK

²¹LIP, IST, FCUL - Av. Elias Garcia, 14-1^o, PT-1000 Lisboa Codex, Portugal

²²Department of Physics, University of Liverpool, P.O. Box 147, Liverpool L69 3BX, UK

²³LPNHE, IN2P3-CNRS, Univ. Paris VI et VII, Tour 33 (RdC), 4 place Jussieu, FR-75252 Paris Cedex 05, France

²⁴Department of Physics, University of Lund, Sölvegatan 14, SE-223 63 Lund, Sweden

²⁵Université Claude Bernard de Lyon, IPNL, IN2P3-CNRS, FR-69622 Villeurbanne Cedex, France

²⁶Univ. d'Aix - Marseille II - CPP, IN2P3-CNRS, FR-13288 Marseille Cedex 09, France

²⁷Dipartimento di Fisica, Università di Milano and INFN, Via Celoria 16, IT-20133 Milan, Italy

²⁸Niels Bohr Institute, Blegdamsvej 17, DK-2100 Copenhagen Ø, Denmark

²⁹NC, Nuclear Centre of MFF, Charles University, Areal MFF, V Holesovickach 2, CZ-180 00, Praha 8, Czech Republic

³⁰NIKHEF, Postbus 41882, NL-1009 DB Amsterdam, The Netherlands

³¹National Technical University, Physics Department, Zografou Campus, GR-15773 Athens, Greece

³²Physics Department, University of Oslo, Blindern, NO-1000 Oslo 3, Norway

³³Dpto. Física, Univ. Oviedo, Avda. Calvo Sotelo s/n, ES-33007 Oviedo, Spain

³⁴Department of Physics, University of Oxford, Keble Road, Oxford OX1 3RH, UK

³⁵Dipartimento di Fisica, Università di Padova and INFN, Via Marzolo 8, IT-35131 Padua, Italy

³⁶Rutherford Appleton Laboratory, Chilton, Didcot OX11 0QX, UK

³⁷Dipartimento di Fisica, Università di Roma II and INFN, Tor Vergata, IT-00173 Rome, Italy

³⁸Dipartimento di Fisica, Università di Roma III and INFN, Via della Vasca Navale 84, IT-00146 Rome, Italy

³⁹DAPNIA/Service de Physique des Particules, CEA-Saclay, FR-91191 Gif-sur-Yvette Cedex, France

⁴⁰Instituto de Física de Cantabria (CSIC-UC), Avda. los Castros s/n, ES-39006 Santander, Spain

⁴¹Dipartimento di Fisica, Università degli Studi di Roma La Sapienza, Piazzale Aldo Moro 2, IT-00185 Rome, Italy

⁴²Inst. for High Energy Physics, Serpukov P.O. Box 35, Protvino, (Moscow Region), Russian Federation

⁴³J. Stefan Institute, Jamova 39, SI-1000 Ljubljana, Slovenia and Department of Astroparticle Physics, School of Environmental Sciences, Kostanjevska 16a, Nova Gorica, SI-5000 Slovenia,

and Department of Physics, University of Ljubljana, SI-1000 Ljubljana, Slovenia

⁴⁴Fysikum, Stockholm University, Box 6730, SE-113 85 Stockholm, Sweden

⁴⁵Dipartimento di Fisica Sperimentale, Università di Torino and INFN, Via P. Giuria 1, IT-10125 Turin, Italy

⁴⁶Dipartimento di Fisica, Università di Trieste and INFN, Via A. Valerio 2, IT-34127 Trieste, Italy

and Istituto di Fisica, Università di Udine, IT-33100 Udine, Italy

⁴⁷Univ. Federal do Rio de Janeiro, C.P. 68528 Cidade Univ., Ilha do Fundão BR-21945-970 Rio de Janeiro, Brazil

⁴⁸Department of Radiation Sciences, University of Uppsala, P.O. Box 535, SE-751 21 Uppsala, Sweden

⁴⁹IFIC, Valencia-CSIC, and D.F.A.M.N., U. de Valencia, Avda. Dr. Moliner 50, ES-46100 Burjassot (Valencia), Spain

⁵⁰Institut für Hochenergiephysik, Österr. Akad. d. Wissensch., Nikolsdorfergasse 18, AT-1050 Vienna, Austria

⁵¹Inst. Nuclear Studies and University of Warsaw, Ul. Hoza 69, PL-00681 Warsaw, Poland

⁵²Fachbereich Physik, University of Wuppertal, Postfach 100 127, DE-42097 Wuppertal, Germany

⁵³On leave of absence from IHEP Serpukhov

⁵⁴Now at University of Florida

1 Introduction

Pairs of photons with missing energy are expected from reactions like $e^+e^- \rightarrow YY$ with the subsequent decay $Y \rightarrow X\gamma$, where X is a neutral undetected particle. Such processes are foreseen in supersymmetric models with gauge-mediated supersymmetry breaking (GMSB) [1–5], where the Y particle can be the lightest neutralino ($\tilde{\chi}_1^0$), decaying to a photon and a gravitino (\tilde{G}). In these models the energy scale of supersymmetry breaking \sqrt{F} is expected to be of the order of 100 – 1000 TeV, much lower than in conventional supergravity models, where it is normally assumed to be around 10^{11} GeV. Since the gravitino mass, $m_{\tilde{G}}$, scales as F/M_P [4], where M_P is the Planck scale, the gravitino can be extremely light, with a mass of the order of 1 keV/ c^2 or lower, and becomes the lightest supersymmetric particle (LSP). In this scenario, the reaction $e^+e^- \rightarrow \tilde{\chi}_1^0\tilde{\chi}_1^0 \rightarrow \tilde{G}\gamma\tilde{G}\gamma$ produces a pair of photons accompanied by two invisible particles. Identical reactions are expected in a “no-scale” supergravity model [6].

If the gravitino mass is larger than 200-300 eV/ c^2 , the $\tilde{\chi}_1^0$ can have a significant lifetime and fly a long distance before decaying, producing photons which do not originate at the beam interaction region. As a consequence, to cover also the extreme case of very large $\tilde{\chi}_1^0$ lifetimes, the search for acoplanar photons from the interaction region needs to be complemented with a search for single photons whose flight direction does not point to the beam interaction region.

Alternatively, in more conventional SUSY models where the $\tilde{\chi}_1^0$ is the LSP, the process $e^+e^- \rightarrow \tilde{\chi}_2^0\tilde{\chi}_2^0 \rightarrow \tilde{\chi}_1^0\gamma\tilde{\chi}_1^0\gamma$ can give rise to similar final states, where the X particle, here identified as $\tilde{\chi}_1^0$, can be relatively heavy [7,8]. In [8] this reaction has been indicated as a possible signal for supersymmetry at LEP in the context of a theoretical framework which could explain several anomalies encountered in different sectors of particle or astroparticle physics, such as the CDF $ee\gamma\gamma$ event [9] and the dark matter problem.

Within the Standard Model, two-photon final states with missing energy are expected from the reaction $e^+e^- \rightarrow \nu\bar{\nu}\gamma\gamma(\gamma)$, for which the dominant diagram corresponds to neutrino production with Z-exchange in the s-channel and double (triple) initial state radiation. Other potential sources of background come from the QED process $e^+e^- \rightarrow \gamma\gamma(\gamma)$, when one photon is lost in a dead region of the detector, and from the $e^+e^- \rightarrow e^+e^-\gamma(\gamma)$ scattering when the electrons are lost or wrongly identified as photons.

This paper describes a search for anomalous production of photon pairs with missing energy based on data collected using the DELPHI detector between 1995 and 1997 at centre-of-mass energies ranging from 130 GeV to 183 GeV. A previous analysis of events with acoplanar photon pairs collected at centre-of-mass energies between 130 and 172 GeV was published in [10] by the DELPHI collaboration. The results described here improve and supersede those of reference [10]. In addition the present search has been complemented with a search for single photons which originate far from the beam interaction region (referred to as “non-pointing single-photon events” in the following). Searches for similar final states have also been performed by the other LEP collaborations [11].

The layout of the paper is as follows: Section 2 summarises the main features of the DELPHI detector, Section 3 describes the real and simulated data samples, Sections 4 to 6 deal with the data analysis. The results are presented in Sections 7 to 9, while in Section 10 some results are interpreted in terms of constraints on the SUSY mass parameters. Section 11 gives the conclusions.

2 The DELPHI detector

A detailed description of the DELPHI detector and its performance can be found in [12]. The present analysis is mainly based on the detection of electromagnetic showers in the High-Density Projection chamber (HPC), in the Forward ElectroMagnetic Calorimeter (FEMC) and in the Small angle Tile Calorimeter (STIC) (which is here used as a veto), as well as on the capability of vetoing events with charged particles using the tracking devices.

Extensive use is made of the fine granularity of the HPC calorimeter, namely $\sim 2 \times 20$ mrad² in $\theta \times \phi$, where θ is the polar angle and ϕ the azimuthal angle, with 9 longitudinal samplings [13], which allows a precise reconstruction of the direction of photon showers.

The outermost layers of the DELPHI Hadron Calorimeter (HAC) are used as a veto in order to reject in-time cosmic events. Off-time cosmic events are efficiently identified and rejected by means of the Cathode-Read-Out (CRO) system of the Hadron Calorimeter tubes.

In addition to the tracks reconstructed in the Time Projection Chamber (TPC), Inner Detector (ID) and Outer Detector (OD), the Vertex Detector (VD) track elements are used in order to reject final states with charged particles coming from the interaction region.

The Vertex Detector was upgraded in 1996: the three layers of silicon strips at radial distances of 6.5 cm, 9 cm and 11 cm from the nominal beam crossing position now fully cover the polar angle region between 25° and 155°.

In addition, two layers of silicon pixels and two layers of ministrips, forming conical surfaces, were added in the two forward regions to form the Very Forward Tracker (VFT) covering angles between 10.5° and 25° to the beam direction [14]. In this region, each particle coming from the beam interaction point crosses at least two silicon layers.

The complete hermeticity (> 99%) for electrons and photons even in the regions not covered by the calorimeters is guaranteed by a set of scintillator counters (Hermeticity Taggers) placed in the polar angle regions around 90° and 40° and at angles corresponding to the thin inactive regions between HPC modules.

3 Real data and simulated samples

3.1 Data samples

The data samples considered in this analysis were collected with the DELPHI detector at the centre-of-mass energies (\sqrt{s}) of 130, 136, 161, 172 and 183 GeV, with corresponding integrated luminosities of 5.9, 5.9, 9.6, 9.9 and 49.7 pb⁻¹ respectively. About one half of the data at $\sqrt{s} = 130$ and 136 GeV were taken in 1995 while the other half was collected in 1997.

The whole data sample was used in the search for acoplanar photon pairs, assuming the photons to originate at the beam interaction point. The samples taken in 1995 at $\sqrt{s} = 130$ GeV and 136 GeV were not considered in the search for non-pointing single-photons as the CRO system of the hadron calorimeter used to reject the background from cosmic rays was not fully operational.

3.2 Simulation of background and signal

Within the Standard Model framework, multiple-photon final states can be produced at LEP via the reactions $e^+e^- \rightarrow \nu\bar{\nu}\gamma\gamma(\gamma)$ and $e^+e^- \rightarrow \gamma\gamma(\gamma)$.

The reaction $e^+e^- \rightarrow \nu\bar{\nu}\gamma\gamma(\gamma)$ corresponds to double photon emission from the initial state electrons, with $\nu\bar{\nu}$ production in the final state. In this case the two photons normally show both large acoplanarity and large acollinearity¹. However, the production cross-section is relatively small in the barrel region of the detector and the photons, being emitted from the initial state particles, tend to have a relatively low transverse momentum with respect to the beam direction. In addition, as the neutrino production is mainly mediated by Z-exchange in the s -channel, the missing mass tends to be close to the Z mass.

The process $e^+e^- \rightarrow \gamma\gamma(\gamma)$ is a QED interaction between the incoming electrons and is mediated by an electron in the t -channel. When only two hard photons are produced, the two photons are necessarily back-to-back and their energy is bound to be exactly equal to the beam energy (E_{beam}). Additional hard photons may be emitted from the initial state particles but these tend to be collinear with the beam direction and are often lost in the beam pipe. When this occurs the visible photon pair can show relatively large acollinearity but small acoplanarity.

Additional minor background contributions can originate from radiative Bhabha ($e^+e^- \rightarrow e^+e^-\gamma(\gamma)$) events when one or two electrons remain undetected or are wrongly identified as photons. Due to the good hermeticity of the DELPHI detector for vetoing high energy electrons, this background can be relevant only in the case where both electrons escape along the beam pipe. However, these events can be eliminated by requiring a minimum transverse missing momentum of the observed photons.

The simulation of the Standard Model background is based on the KORALZ generator [15] for the $e^+e^- \rightarrow \nu\bar{\nu}\gamma\gamma(\gamma)$ reaction, on the RADCOR model [16] for the $e^+e^- \rightarrow \gamma\gamma(\gamma)$ reaction and on BABAMC [17] for Bhabha events. The equivalent integrated luminosity for the main $e^+e^- \rightarrow \nu\bar{\nu}\gamma\gamma(\gamma)$ background exceeds 100 times the recorded data statistics at each centre-of-mass energy.

In signal events the photons have a flat distribution in $\cos\theta$ and in energy, with minimum and maximum energies which depend on the masses of the particles involved in the reaction (and on the centre-of-mass energy). The simulation of the kinematics of the signal for the reaction $e^+e^- \rightarrow YY \rightarrow X\gamma X\gamma$ was performed with the SUSYGEN Monte Carlo program [18], which generates processes of the type $e^+e^- \rightarrow \tilde{\chi}_1^0\tilde{\chi}_1^0 \rightarrow \tilde{G}\gamma\tilde{G}\gamma$ and $e^+e^- \rightarrow \tilde{\chi}_2^0\tilde{\chi}_2^0 \rightarrow \tilde{\chi}_1^0\gamma\tilde{\chi}_1^0\gamma$. Samples of the process $e^+e^- \rightarrow \tilde{\chi}_1^0\tilde{\chi}_1^0 \rightarrow \tilde{G}\gamma\tilde{G}\gamma$ in the case of non-negligible $\tilde{\chi}_1^0$ lifetime were also generated with SUSYGEN.

The features of signal and background, as predicted by simulations, justify the selection criteria presented in the following section. Two independent analyses were performed for the case of short-lived and long-lived Y particles.

1. For short-lived Y particles two acoplanar photons were searched for. This analysis is sensitive to mean decay paths of the order of 1 metre or shorter.
2. For the case of long-lived Y particles a search was performed for single photons with a reconstructed shower axis which does not point to the beam interaction region. This second analysis is sensitive to relatively large mean decay paths on the detector scale (from 1 to some 20 metres).

¹Throughout this paper the acollinearity and acoplanarity are defined to be zero when the two photons are back-to-back in space and in the transverse plane, respectively.

4 Event selection for short-lived Y particles

The search for $e^+e^- \rightarrow YY \rightarrow X\gamma X\gamma$ events with prompt Y decay was based on a two-step procedure.

First events with two energetic photons and missing transverse energy were selected. This preselection was used in order to monitor the modelling of the Standard Model process $e^+e^- \rightarrow \nu\bar{\nu}\gamma\gamma(\gamma)$ which dominates the expected background.

In a second step the signal was enhanced over the background by requirements for missing mass, transverse momentum or polar angle. This second step depends on the assumption about the X particle, which can be extremely light (as in the case of the gravitino in GMSB models) or relatively heavy (as the $\tilde{\chi}_1^0$ in the SUSY scenario considered in [8]).

4.1 Event preselection

The preselection of two-photon final states was based on the following requirements:

- at least two electromagnetic clusters detected in the HPC or FEMC, each with polar angle in the region $10^\circ < \theta_\gamma < 170^\circ$ and scaled energy $x_\gamma = E_\gamma/E_{beam} > 0.05$;
- at least one electromagnetic cluster satisfying the previous condition with polar angle in the region $25^\circ < \theta_\gamma < 155^\circ$;
- no showers in the external layers of the HAC calorimeter;
- no tracks reconstructed in the VD or VFT detectors corresponding to any electromagnetic cluster in HPC and FEMC or to any charged particle track reconstructed by the ID-TPC-OD system;
- acoplanarity of the two most energetic photons $> 3^\circ$;
- acoplanarity of the two most energetic photons $< 140^\circ$ when $\Delta\theta = |\theta_{\gamma 1} - \theta_{\gamma 2}| < 20^\circ$;
- total visible energy $E_{vis} < 0.9\sqrt{s}$;
- total transverse momentum $p_T > 0.03E_{miss}$, where $E_{miss} = \sqrt{s} - E_{vis}$;
- polar angle of the missing momentum in the region $10^\circ < \theta_{miss} < 170^\circ$;
- no isolated hits in the Hermeticity Taggers;
- total energy in the STIC (E_{STIC}) below $0.02\sqrt{s}$.

The clusters in the HPC and FEMC are defined as energy deposits where all small showers in a cone of 10° (half-angle) around the main shower have been merged together. In the HPC the photon clusters must meet the following criteria, in order to reject small clusters produced by alpha particles emitted from the lead converter and by the electronic noise:

- some energy deposit should be present in at least four of the nine longitudinal layers;
- no more than one empty layer is allowed along the longitudinal shower development;
- the energy deposited in any single layer must be less than 90% of the total cluster energy;
- the reconstructed shower axis should point to the beam interaction region within 25° in the θ and ϕ projections.

The use of the VD alone to veto charged particle tracks avoids the rejection of photons converting behind the silicon tracker. By vetoing energy deposits in the external layers of the HAC, in-time cosmic events are rejected. The acoplanarity requirement reduces the contamination from $e^+e^- \rightarrow \gamma\gamma$ events, while the combined requirement on acoplanarity and $\Delta\theta$ eliminates single-photon events with the photon converting in the material in

front of the calorimeters and producing two separate clusters in the FEMC or HPC. Finally, the requirement on the total missing momentum together with the adoption of the STIC veto in the very forward region eliminate the background of doubly radiative Bhabha events where the electrons escape detection along the beam pipe.

Events with three electromagnetic clusters passing the previous selection were retained only if they satisfied the additional constraints:

- $E_{vis} < 0.8\sqrt{s}$;
- the event is significantly aplanar, i.e., the sum of the angles formed by the three observed photons is less than 358° .

Events with four or more electromagnetic clusters were rejected.

These additional requirements remove QED $e^+e^- \rightarrow \gamma\gamma(\gamma)$ events with more than two photons without reducing the signal efficiency when an additional photon is radiated.

As already stated, this preselection was used in order to monitor the modelling and simulation of the Standard Model background. In order to improve the signal-to-background ratio the preselected events were then subjected to stricter requirements depending on the physics scenario considered for the signal as described in the next sections.

4.2 Final candidate selection: case of a massless X particle

For the special case of a (practically) massless X particle as in the reaction $e^+e^- \rightarrow \tilde{\chi}_1^0 \tilde{\chi}_1^0 \rightarrow \tilde{G}\gamma\tilde{G}\gamma$ the following constraints were imposed:

- the scaled transverse momentum of each cluster, $x_\gamma^T = p_\gamma^T/E_{beam}$, should exceed 0.07 if the measured missing mass (M_{miss}) is larger than $60 \text{ GeV}/c^2$ and should exceed 0.14 in the special mass region $80 \text{ GeV}/c^2 < M_{miss} < 110 \text{ GeV}/c^2$;
- the energies and angles of the detected photons must be compatible with those expected for a given $Y = \tilde{\chi}_1^0$ mass.

The first requirement strongly suppresses the Standard Model background, where the photons, being emitted from the initial state particles, have a relatively low transverse momentum with respect to the beam direction. A more severe requirement is used when the missing mass is close to the Z mass because this is the kinematic region favoured by the $e^+e^- \rightarrow \nu\bar{\nu}\gamma\gamma(\gamma)$ process.

4.3 Final candidate selection: case of a massive X particle

For the more general reaction $e^+e^- \rightarrow YY \rightarrow X\gamma X\gamma$, where the X particle is massive, the following criteria were imposed:

- the polar angle of each photon should always belong to the interval $[20^\circ, 160^\circ]$ if $M_{miss} > 60 \text{ GeV}/c^2$ and should satisfy $40^\circ < \theta_\gamma < 140^\circ$ in the special case that $80 \text{ GeV}/c^2 < M_{miss} < 110 \text{ GeV}/c^2$;
- the measured energies of the detected photons must be compatible with those expected for a given pair of $Y = \tilde{\chi}_2^0$ and $X = \tilde{\chi}_1^0$ masses.

The first criterion is justified by the fact that, for a small mass difference between the Y particle and the X particle, the expected photon energies and transverse momenta can be relatively small and cannot be used to discriminate against the background. In this case the event selection can only be based on the photon polar angle distribution $d\sigma/d\cos\theta$, which is flat for the signal and peaked in the forward direction for the background.

5 Event selection for long-lived Y particles

When the gravitino mass exceeds a few tens of electron volts the decay $\tilde{\chi}_1^0 \rightarrow \tilde{G}\gamma$ can have a non-negligible lifetime and the photons can originate from points relatively far from the beam interaction region.

For long average decay distances ($d > 4$ m) the probability to detect both photons from the $e^+e^- \rightarrow \tilde{\chi}_1^0\tilde{\chi}_1^0 \rightarrow \tilde{G}\gamma\tilde{G}\gamma$ reaction becomes very small and therefore, in order to ensure a large sensitivity for the signal, events with a single non-pointing photon have to be searched for. By imposing that the shower axes of single-photon candidates do not point at the beam interaction region, the otherwise overwhelming background of $e^+e^- \rightarrow \nu\bar{\nu}\gamma$ events can be strongly reduced.

The selection of non-pointing single photon events was based on the following requirements:

- only one electromagnetic cluster with $E_\gamma > 10$ GeV and $45^\circ < \theta_\gamma < 135^\circ$, where θ_γ is the angle formed by the beam line and the straight line passing through the beam spot and the photon shower barycentre, should be present in the event;
- the HPC photon clusters should satisfy the requirements described in Section 4.1, with the exception of the requirement concerning the reconstructed shower axis direction; in addition some energy deposit must be present in at least one of the three innermost longitudinal layers and the radial depth of the shower barycentre should not exceed 35 cm from the HPC inner radius;
- the minimum distance (impact parameter) between the beam crossing point and the shower axis reconstructed in the HPC should be greater than 40 cm.
- no tracks pointing at the electromagnetic cluster should be present in the Vertex Detector;
- no track should be reconstructed in the other tracking devices;
- no isolated hit should be present in the hermeticity taggers;
- no energy deposit should be present in the external layers of the Hadron Calorimeter;
- no tracks should be reconstructed by the Hadron Calorimeter Cathode-Read-Out system.

Compared with the HPC cluster definition described in Section 4.1, the cluster selection criteria have been strengthened slightly in order to eliminate the contamination from noise and cosmic events which is expected to be larger for single-photon events than for photon pairs. The additional requirement on the shower impact parameter as reconstructed by the HPC provides a reduction of the Standard Model $e^+e^- \rightarrow \nu\bar{\nu}\gamma$ background by a factor 140, according to the simulation.

6 Signal efficiency

The signal efficiency was determined by simulating the process $e^+e^- \rightarrow YY \rightarrow X\gamma X\gamma$ for Y masses between 45 GeV/ c^2 and the kinematic limit and for X masses between 0 and m_Y with 5 GeV/ c^2 intervals at each centre-of-mass energy. Due to the extreme simplicity of the final states, the simulation of the detector performance was based on a simple Monte Carlo program. For nine different combinations of the X and Y masses, these estimates were cross-checked with a full simulation of the DELPHI detector as provided by the DELSIM [12] package and were found to be correct within 4% (relative).

The trigger efficiency for single photons was studied in detail as a function of energy, polar angle and time, by using an independent track trigger for isolated electrons. The

trigger efficiency for two-photon final states was derived from the single-photon trigger efficiency as estimated from the data, taking into account the energy, the polar angle and the running period, assuming each photon to be independent from the others. The total efficiency for the signal was estimated as the product of the selection and trigger efficiencies.

The signal efficiency (including the trigger contribution) for the case $m_X = m_{\tilde{G}} \approx 0$ is shown in Figure 1 for the various centre-of-mass energies as a function of $m_Y = m_{\tilde{\chi}_1^0}$, where the Y particle is assumed to decay at the beam interaction point. The signal sensitivity is lower in the data taken at $\sqrt{s} = 172$ GeV due to a temporary malfunctioning of the barrel photon trigger in 1996.

In the more general case that the undetected X particles are massive, the signal efficiency at $\sqrt{s} = 183$ GeV is shown in Figure 2, where the Y and X particles have been identified with $\tilde{\chi}_2^0$ and $\tilde{\chi}_1^0$ respectively in the process $e^+e^- \rightarrow \tilde{\chi}_2^0\tilde{\chi}_2^0 \rightarrow \tilde{\chi}_1^0\gamma\tilde{\chi}_1^0\gamma$. Similar curves were obtained at lower centre-of-mass energies. Due to the requirement of a minimum photon energy adopted in the event selection, the signal sensitivity becomes small when the mass difference $\Delta m = m_Y - m_X$ is below 5-10 GeV/ c^2 . The Y particle is assumed to decay at the beam interaction point.

The selection efficiency in the search for single, non-pointing photons for the $e^+e^- \rightarrow \tilde{\chi}_1^0\tilde{\chi}_1^0 \rightarrow \tilde{G}\gamma\tilde{G}\gamma$ channel at $\sqrt{s}=183$ GeV is shown in Figure 3 as a function of the neutralino mean decay path for $m_{\tilde{\chi}_1^0} = 60$ GeV/ c^2 and $m_{\tilde{\chi}_1^0} = 80$ GeV/ c^2 . The same figure also shows the efficiency obtained when the event selection described in Section 4.2 is applied to the search for long-lived neutralinos. The efficiency has been obtained from a suitable parametrisation which has been fitted to samples of fully simulated events based on the DELSIM package with five neutralino mean decay paths, namely 1, 2, 4, 6 and 8 metres.

7 Results of the search for short-lived Y particles

7.1 Standard Model background monitoring

The data samples obtained after preselecting two-photon events are described in Table 1. In Figure 4 the missing mass distribution is compared with the KORALZ expectations after summing up the samples from all centre-of-mass energies. The contribution of the other background sources was estimated to be below 0.2 events in total and has been neglected.

A good agreement was found between the observed data and the background simulation. Summing up all data samples, ten events were found, while 10.2 events were expected from the Standard Model background.

Figure 5 shows the difference in angle (for the θ and ϕ projections) between the direction of the HPC shower axis and the straight line passing through the photon shower barycentre and the beam interaction region as observed in all photons detected by the HPC belonging to the preselected sample. All HPC photons appear to originate in the proximity of the beam interaction region. The figure demonstrates the good HPC resolution in reconstructing the photon flight direction.

As mentioned in Section 4 the two-photon events described in Table 1 were passed through a tighter selection in order to enhance the signal-to-background ratio.

Year	\sqrt{s} (GeV)	$\int \mathcal{L}$ (pb $^{-1}$)	Data	$e^+e^- \rightarrow \nu\bar{\nu}\gamma\gamma(\gamma)$
1995	130	2.92	0	0.73 ± 0.02
1995	136	3.01	0	0.70 ± 0.02
1996	161	9.58	1	1.39 ± 0.03
1996	172	9.85	3	1.09 ± 0.03
1997	130	3.05	0	0.77 ± 0.02
1997	136	2.91	0	0.68 ± 0.02
1997	183	49.73	6	4.78 ± 0.12
Total	130-183	81.05	10	10.15 ± 0.13

Table 1: The year of data taking, the centre-of-mass energy, the integrated luminosity, the number of events passing the preselection of two-photon events with missing energy and the number of background events expected in the Standard Model.

7.2 Case of massless X particles

For the $m_X \approx 0$ case the number of events found in the data after applying the transverse momentum requirement in Section 4.2 is compared to the $e^+e^- \rightarrow \nu\bar{\nu}\gamma\gamma(\gamma)$ background expectations in Figure 6 as a function of the measured missing mass. The number of detected events at each centre-of-mass energy is described in Table 2, together with the corresponding background estimates. No excess was seen in the data, as two events were found while 2.7 were expected from Standard Model sources. The two data candidates, both taken at $\sqrt{s} = 172$ GeV, are the same as those identified in a previous analysis [10]. No candidate has been found at $\sqrt{s} = 183$ GeV, where a background of 1.65 events was expected.

\sqrt{s} (GeV)	Data	$e^+e^- \rightarrow \nu\bar{\nu}\gamma\gamma(\gamma)$
130	0	0.17 ± 0.01
136	0	0.15 ± 0.01
161	0	0.36 ± 0.02
172	2	0.33 ± 0.02
183	0	1.65 ± 0.08
Total	2	2.66 ± 0.11

Table 2: The number of candidates found in the data and expected from the $e^+e^- \rightarrow \nu\bar{\nu}\gamma\gamma(\gamma)$ background as a function of the centre-of-mass energy. The results correspond to the search for the reaction $e^+e^- \rightarrow YY \rightarrow X\gamma X\gamma$ where the X particle is practically massless.

The most relevant features of the two acoplanar-photon candidates are described in Table 3. Of the two candidates only one is compatible with Y masses above 78 GeV/ c^2 . Neither candidate is compatible with Y masses larger than 86 GeV/ c^2 as they were found in the data sample collected at $\sqrt{s} = 172$ GeV.

\sqrt{s} (GeV)	$E_{\gamma 1}$ (GeV)	$E_{\gamma 2}$ (GeV)	$\theta_{\gamma 1}$ ($^{\circ}$)	$\theta_{\gamma 2}$ ($^{\circ}$)	M_{miss} (GeV/ c^2)	$M_{\tilde{\chi}_1^0}^{max}$ (GeV/ c^2)
172	39.2	29.0	127.2	28.9	94.1	86.0
172	27.6	13.9	97.2	134.7	126.0	78.0

Table 3: The relevant features (photon energies, photon polar angles and missing mass) of the candidate events found in the search for the reaction $e^+e^- \rightarrow YY \rightarrow X\gamma X\gamma$, in the case of a massless X particle.

7.3 Case of massive X particles

In the analysis optimised for a massive X particle, four events were found in total in the data after applying the cut on the photon polar angles described in Section 4.3, while 3.4 were expected on the basis of the background simulation. The distribution of the data candidates among the centre-of-mass energies is described in Table 4, while the missing mass distribution of the total sample is plotted in Figure 7 together with the prediction from the KORALZ model. The photon energies, polar angles and missing mass of the four data events are described in Table 5. All four events have features consistent with the expected background.

\sqrt{s} (GeV)	Data	$e^+e^- \rightarrow \nu\bar{\nu}\gamma\gamma(\gamma)$
130	0	0.38 ± 0.02
136	0	0.35 ± 0.02
161	0	0.45 ± 0.03
172	1	0.36 ± 0.02
183	3	1.85 ± 0.09
Total	4	3.39 ± 0.13

Table 4: The number of candidates found in the data and expected from the $e^+e^- \rightarrow \nu\bar{\nu}\gamma\gamma(\gamma)$ background as a function of the centre-of-mass energy. The results correspond to the search for the reaction $e^+e^- \rightarrow YY \rightarrow X\gamma X\gamma$ where the X particle is massive.

\sqrt{s} (GeV)	$E_{\gamma 1}$ (GeV)	$E_{\gamma 2}$ (GeV)	$\theta_{\gamma 1}$ ($^{\circ}$)	$\theta_{\gamma 2}$ ($^{\circ}$)	M_{miss} (GeV/ c^2)
172	27.6	13.9	97.2	134.7	126.0
183	43.9	6.2	25.3	70.9	124.4
183	71.8	7.6	59.7	30.1	72.8
183	14.3	14.0	120.5	24.9	154.6

Table 5: The relevant features (photon energies, photon polar angles and missing mass) of the candidate events found in the search for the reaction $e^+e^- \rightarrow YY \rightarrow X\gamma X\gamma$, in the case of a massive X particle.

8 Results of the search for long-lived Y particles

In the Standard Model no background is expected from photonic events when the photons do not originate from the beamspot. However, in some rare cases the direction of the photon shower axis can be wrongly reconstructed in the HPC, faking a signal event. This probability was studied with detailed Monte Carlo simulations according to which 0.9 ± 0.3 events with reconstructed photon impact parameter greater than 40 cm are expected from the $e^+e^- \rightarrow \nu\bar{\nu}\gamma$ process in the total analysed sample at $\sqrt{s}=130\text{--}183$ GeV. The fraction of this background affecting each subsample is proportional to the corresponding integrated luminosity divided by the beam energy squared.

The background from cosmic rays leaving no sign in the tracking devices, in the outermost layers of the Hadron Calorimeter or in the Cathode-Read-Out system is estimated to be negligible.

Two events with non-pointing single photons were found in the data, both at $\sqrt{s} = 161$ GeV, in agreement with the total expected background. The most relevant features of the two candidate events are described in Table 6.

The first event has an impact parameter of 40.8 cm, which is just above the minimum required, and a measured missing mass of $92.2 \text{ GeV}/c^2$, close to the Z mass. As a consequence this event may safely be interpreted as residual $e^+e^- \rightarrow \nu\bar{\nu}\gamma$ background. The second event presents a lower missing mass ($74.2 \text{ GeV}/c^2$) but is also compatible with being an event of neutrino-antineutrino production with initial state radiation in which the photon shower axis has been wrongly determined due to the presence of a calorimeter crack.

\sqrt{s} (GeV)	$E_{\gamma 1}$ (GeV)	$\theta_{\gamma 1}$ ($^\circ$)	M_{miss} (GeV/ c^2)	imp. par. (cm)
161	54.1	107.5	92.2	40.8
161	63.4	49.3	74.2	120.3

Table 6: The relevant features (photon energy, polar angle, missing mass and impact parameter) of the two candidate events found in the search for non-pointing single-photons.

9 Limits on the signal cross-section

Since no evidence for a signal was found in the data, cross-section limits for the process $e^+e^- \rightarrow YY$, followed by $Y \rightarrow X\gamma$, were derived for each considered centre-of-mass energy and any X,Y mass combination for the case of short-lived Y particles (with mean decay path shorter than about one metre).

For the case of a massless X particle, or equivalently for the reaction $e^+e^- \rightarrow \tilde{\chi}_1^0\tilde{\chi}_1^0 \rightarrow \tilde{G}\gamma\tilde{G}\gamma$, the limits obtained are shown in Figure 8. These are expressed in terms of 95% confidence level upper limits on the signal cross-section $\sigma(e^+e^- \rightarrow \tilde{\chi}_1^0\tilde{\chi}_1^0)$ at each centre-of-mass energy as a function of the $\tilde{\chi}_1^0$ mass. In particular, the upper limit on the signal cross-section at the highest centre-of-mass energy ($\sqrt{s} = 183$ GeV) ranges between 0.13 and 0.10 pb, depending on the $\tilde{\chi}_1^0$ mass. A total systematic uncertainty of $\pm 5\%$ was assumed for the signal efficiency, which includes the uncertainties on the signal simulation (4%) and on the trigger efficiency (3%). This was taken into account in deriving the cross-section limits according to the formula in [19]. The effect of the

systematic error on the cross-section limits is negligible. The decay $\tilde{\chi}_1^0 \rightarrow \tilde{G}\gamma$ is assumed to occur with 100% branching ratio.

Figure 9 shows the 95% confidence level upper limit on $\sigma(e^+e^- \rightarrow \tilde{\chi}_1^0\tilde{\chi}_1^0)$ at $\sqrt{s} = 183$ GeV when the results obtained from all data samples are combined according to the likelihood ratio multichannel method [20] assuming that the signal cross-section scales as β_Y^3/s . If the cross-section is assumed to scale as β_Y/s , rather than β_Y^3/s , the limit shown in Figure 9 decreases by as much as 10%.

Similarly, the results obtained in the search for the process $e^+e^- \rightarrow \tilde{\chi}_2^0\tilde{\chi}_2^0 \rightarrow \tilde{\chi}_1^0\gamma\tilde{\chi}_1^0\gamma$ are shown in Figures 10 and 11, in terms of 95% confidence level upper limits on the signal cross-section. The limits are shown as a function of the mass difference between $\tilde{\chi}_2^0$ and $\tilde{\chi}_1^0$ at each centre-of-mass energy. As in the previous case, the decay $\tilde{\chi}_2^0 \rightarrow \tilde{\chi}_1^0\gamma$ is assumed to occur in proximity of the beam interaction point, with 100% branching ratio.

The upper limit on the signal cross-section at $\sqrt{s} = 183$ GeV as derived from all data samples is shown in Figure 12, where β_Y^3/s scaling of the cross-section has been assumed.

The cross-section limits obtained in the search for the process $e^+e^- \rightarrow \tilde{\chi}_1^0\tilde{\chi}_1^0 \rightarrow \tilde{G}\gamma\tilde{G}\gamma$ when $\tilde{\chi}_1^0$ has a finite and detectable lifetime are shown in Figure 13 as a function of the $\tilde{\chi}_1^0$ mean decay path. The limits are displayed for $m_{\tilde{\chi}_1^0} = 60$ GeV/ c^2 and $80 < m_{\tilde{\chi}_1^0} < 91$ GeV/ c^2 after combining the data at all centre-of-mass energies. The curves correspond to the results obtained when the selections of Section 4.2 and Section 5 are applied to the data, first separately and then combined according to [20].

10 Supersymmetry interpretation of the results

The limits obtained in terms of neutralino production cross-sections can be interpreted in the context of Supersymmetric Models to constrain the free parameters of the theory.

By comparing the cross-section limits for the process $e^+e^- \rightarrow \tilde{\chi}_1^0\tilde{\chi}_1^0$ at $\sqrt{s} = 183$ GeV with the expectations of the GMSB model considered in [5] where the neutralino is pure Bino (\tilde{B}) and $m_{\tilde{\epsilon}_R} = 1.1 m_{\tilde{\chi}_1^0}$, the lower limit of 83 GeV/ c^2 at 95% confidence level is derived on the lightest neutralino mass. This constraint does not depend significantly on the \tilde{e}_L mass.

The region excluded by DELPHI data in the $m_{\tilde{\chi}_1^0}$ versus $m_{\tilde{\epsilon}_R}$ plane is shown in Figure 14, where it is compared with the region compatible with the \tilde{e} interpretation of the $e\bar{e}\gamma\gamma$ CDF event [9] (as taken from [21]).

In GMSB models, the neutralino lifetime in the decay $\tilde{\chi}_1^0 \rightarrow \tilde{G}\gamma$ strongly depends on the gravitino mass $m_{\tilde{G}}$, which in turn is related to the scale \sqrt{F} according to [4]:

$$m_{\tilde{G}} = \frac{F}{\sqrt{3}M_P} \sim 2.5 \left(\frac{\sqrt{F}}{100 \text{ TeV}} \right)^2 \text{ eV}/c^2. \quad (1)$$

The neutralino lifetime in the process $e^+e^- \rightarrow \tilde{\chi}_1^0\tilde{\chi}_1^0 \rightarrow \tilde{G}\gamma\tilde{G}\gamma$ is then given by:

$$c\tau = 130 \left(\frac{m_{\tilde{\chi}_1^0}}{100 \text{ GeV}} \right)^{-5} \left(\frac{\sqrt{F}}{100 \text{ TeV}} \right)^4 \mu\text{m}. \quad (2)$$

By taking into account the variation of the upper limit on $\sigma(e^+e^- \rightarrow \tilde{\chi}_1^0\tilde{\chi}_1^0 \rightarrow \tilde{G}\gamma\tilde{G}\gamma)$ with the neutralino lifetime, lower bounds can be set on the scale \sqrt{F} . These are shown in Figure 15 as a function of the neutralino mass for the hypothesis that the neutralino is pure Bino (\tilde{B}) and $m_{\tilde{\epsilon}_R} = 1.1 m_{\tilde{\chi}_1^0}$.

11 Conclusions

The search for anomalous production of acoplanar photon pairs which could be produced by the reaction $e^+e^- \rightarrow YY$ followed by $Y \rightarrow X\gamma$, where X is an undetected particle, yielded negative results in the data collected by DELPHI at the centre-of-mass energies ranging between 130 and 183 GeV, for any combination of the X and Y masses. The hypothesis of a Y particle with large lifetime was also considered. The number and the features of the selected events in the data were found to be compatible with the expected background.

On the basis of these results upper limits in the range 0.10-0.13 pb can be set on the $e^+e^- \rightarrow \tilde{\chi}_1^0\tilde{\chi}_1^0$ cross-section at $\sqrt{s} = 183$ GeV assuming the decay $\tilde{\chi}_1^0 \rightarrow \tilde{G}\gamma$ to have 100% probability and negligible lifetime. This implies $m_{\tilde{\chi}_1^0} > 83$ GeV/ c^2 in GMSB models with $m_{\tilde{\varepsilon}_R} = 1.1 m_{\tilde{\chi}_1^0}$ and $\tilde{\chi}_1^0 \approx \tilde{B}$. If the constraint on the $\tilde{\chi}_1^0 \rightarrow \tilde{G}\gamma$ lifetime is relaxed, a lower limit of 1000 TeV (650 TeV) can be set on the SUSY breaking scale \sqrt{F} for $m_{\tilde{\chi}_1^0} \sim 80$ GeV/ c^2 ($m_{\tilde{\chi}_1^0} \sim 45$ GeV/ c^2).

Similarly, upper limits varying from 0.10 pb to 0.25 pb depending on the $\tilde{\chi}_1^0$ and $\tilde{\chi}_2^0$ masses were set on the production cross-section for the process $e^+e^- \rightarrow \tilde{\chi}_1^0\tilde{\chi}_1^0 \rightarrow \tilde{G}\gamma\tilde{G}\gamma$ at $\sqrt{s} = 183$ GeV.

Acknowledgements

We are greatly indebted to our technical collaborators, to the members of the CERN-SL Division for the excellent performance of the LEP collider, and to the funding agencies for their support in building and operating the DELPHI detector.

We acknowledge in particular the support of

Austrian Federal Ministry of Science and Traffics, GZ 616.364/2-III/2a/98,

FNRS-FWO, Belgium,

FINEP, CNPq, CAPES, FUJB and FAPERJ, Brazil,

Czech Ministry of Industry and Trade, GA CR 202/96/0450 and GA AVCR A1010521,

Danish Natural Research Council,

Commission of the European Communities (DG XII),

Direction des Sciences de la Matière, CEA, France,

Bundesministerium für Bildung, Wissenschaft, Forschung und Technologie, Germany,

General Secretariat for Research and Technology, Greece,

National Science Foundation (NWO) and Foundation for Research on Matter (FOM),

The Netherlands,

Norwegian Research Council,

State Committee for Scientific Research, Poland, 2P03B06015, 2P03B03311 and SPUB/P03/178/98,

JNICT-Junta Nacional de Investigação Científica e Tecnológica, Portugal,

Vedecka grantova agentura MS SR, Slovakia, Nr. 95/5195/134,

Ministry of Science and Technology of the Republic of Slovenia,

CICYT, Spain, AEN96-1661 and AEN96-1681,

The Swedish Natural Science Research Council,

Particle Physics and Astronomy Research Council, UK,

Department of Energy, USA, DE-FG02-94ER40817.

References

- [1] P. Fayet, Phys. Lett. **B69** (1977) 489;
P. Fayet, Phys. Lett. **B70** (1977) 461.
- [2] J. Ellis and J.S. Hagelin, Phys. Lett. **B122** (1983) 303.
- [3] S. Ambrosanio et al., Phys. Rev. **D54** (1996) 5395.
- [4] S. Dimopoulos et al., Phys. Rev. Lett. **76** (1996) 3494;
S. Dimopoulos et al., Phys. Rev. **D54** (1996) 3283.
- [5] S. Dimopoulos, S. Thomas and J.D. Wells, Nucl. Phys. **B488** (1997) 39.
- [6] J.L. Lopez et al., Phys. Rev. **D49** (1994) 343;
J.L. Lopez et al., Int. J. Mod. Phys. **A10** (1995) 4241;
J.L. Lopez and D.V. Nanopoulos, Mod. Phys. Lett. **A11** (1996) 2473;
J.L. Lopez, D.V. Nanopoulos, A. Zichichi, Phys. Rev. Lett. **77** (1996) 5168.
- [7] S. Ambrosanio et al., Phys. Rev. Lett. **76** (1996) 3498;
S. Ambrosanio et al., Phys. Rev. **D55** (1997) 1392;
H.E. Haber and D. Wyler, Nucl. Phys. **B323** (1989) 267.
- [8] G.L. Kane and G. Mahlon, Phys. Lett. **B408** (1997) 222.
- [9] CDF Collaboration, F. Abe et al., hep-ex/9801019, Fermilab-Pub-98-024-E, Phys. Rev. Lett. **81** (1998) 1791.
- [10] DELPHI Collaboration, P. Abreu et al., E. Phys. J. **C1** (1998) 1.
- [11] ALEPH Collaboration, R. Barate et al., Phys. Lett. **B429** (1998) 201;
L3 Collaboration, M. Acciarri et al., Phys. Lett. **B415** (1997) 299;
OPAL Collaboration, K. Ackerstaff et al., E. Phys. J. **C2** (1998) 607.
- [12] DELPHI Collaboration, P. Aarnio et al., Nucl. Inst. and Meth. **A303** (1991) 233;
DELPHI Collaboration, P. Abreu et al., Nucl. Inst. and Meth. **A378** (1996) 57.
- [13] A. Algeri et al., IEEE Trans. Nucl. Sci. **42** (1984) 491.
- [14] A. Andreazza et al., Nucl. Inst. and Meth. **A367** (1995) 198.
- [15] S. Jadach et al., Comp. Phys. Comm. **66** (1991) 276.
- [16] F.A. Berends et al., Nucl. Phys. **B61** (1973) 414;
F.A. Berends et al., Nucl. Phys. **B186** (1981) 22;
F.A. Berends et al., Nucl. Phys. **B239** (1984) 395.
- [17] F.A. Berends, W. Hollik and R. Kleiss, Nucl. Phys. **B304** (1988) 712.
- [18] S. Katsanevas and P. Morawitz, hep-ph/9711417, submitted to Comp. Phys. Comm.
- [19] R.D. Cousins and V.L. Highland, Nucl. Inst. and Meth. **A320** (1992) 331.
- [20] A. Read, DELPHI 97-158 PHYS 737.
- [21] J.L. Lopez and D. Nanopoulos, Phys. Rev. **D55** (1997) 4450.

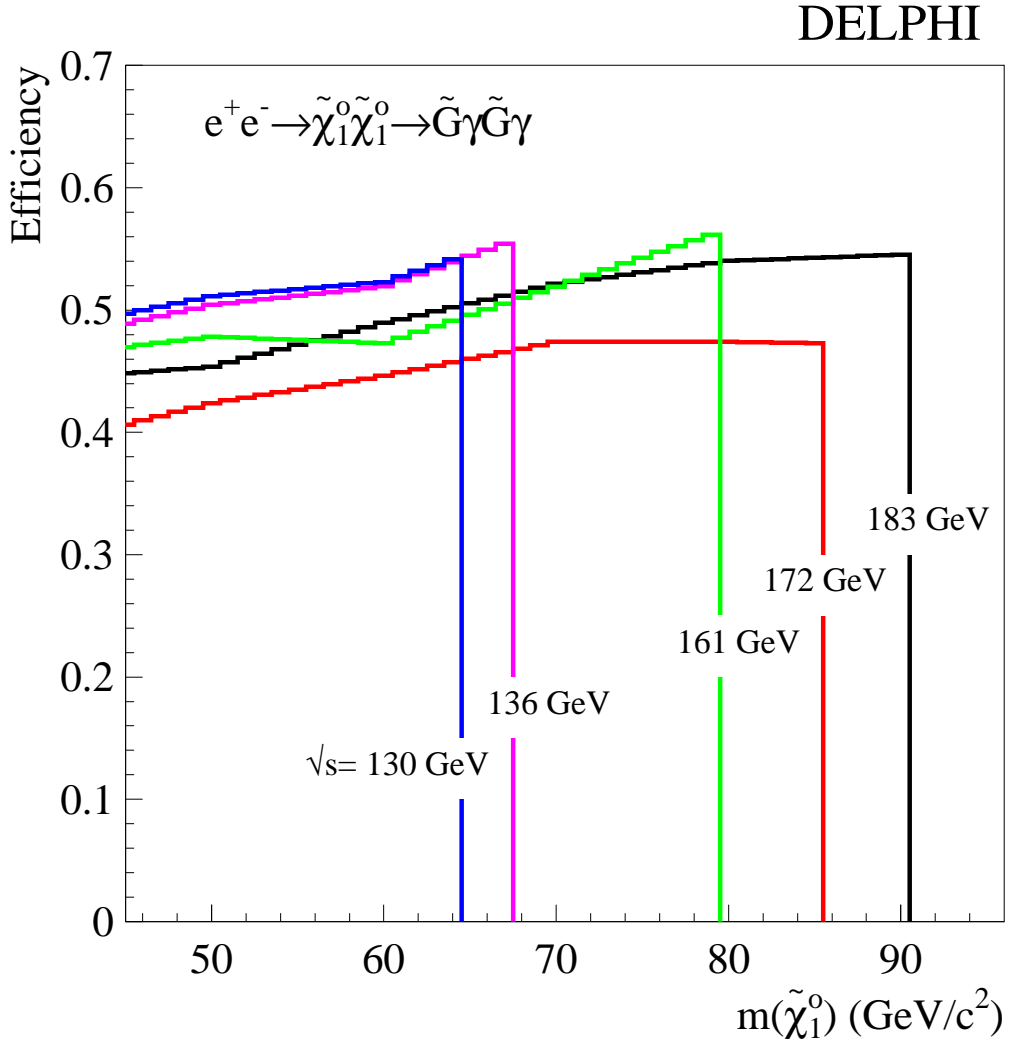


Figure 1: Efficiency for the process $e^+e^- \rightarrow \tilde{\chi}_1^0 \tilde{\chi}_1^0 \rightarrow \tilde{G}\gamma\tilde{G}\gamma$ in GMSB models as a function of the $\tilde{\chi}_1^0$ mass at various centre-of-mass energies. The efficiencies apply for any generic $e^+e^- \rightarrow YY \rightarrow X\gamma X\gamma$ reaction with the massless X particle remaining undetected. The efficiency includes contributions from the trigger and the selections described in Section 4, including the requirement of kinematic compatibility between the selected events and the signal for each given $Y=\tilde{\chi}_1^0$ mass.

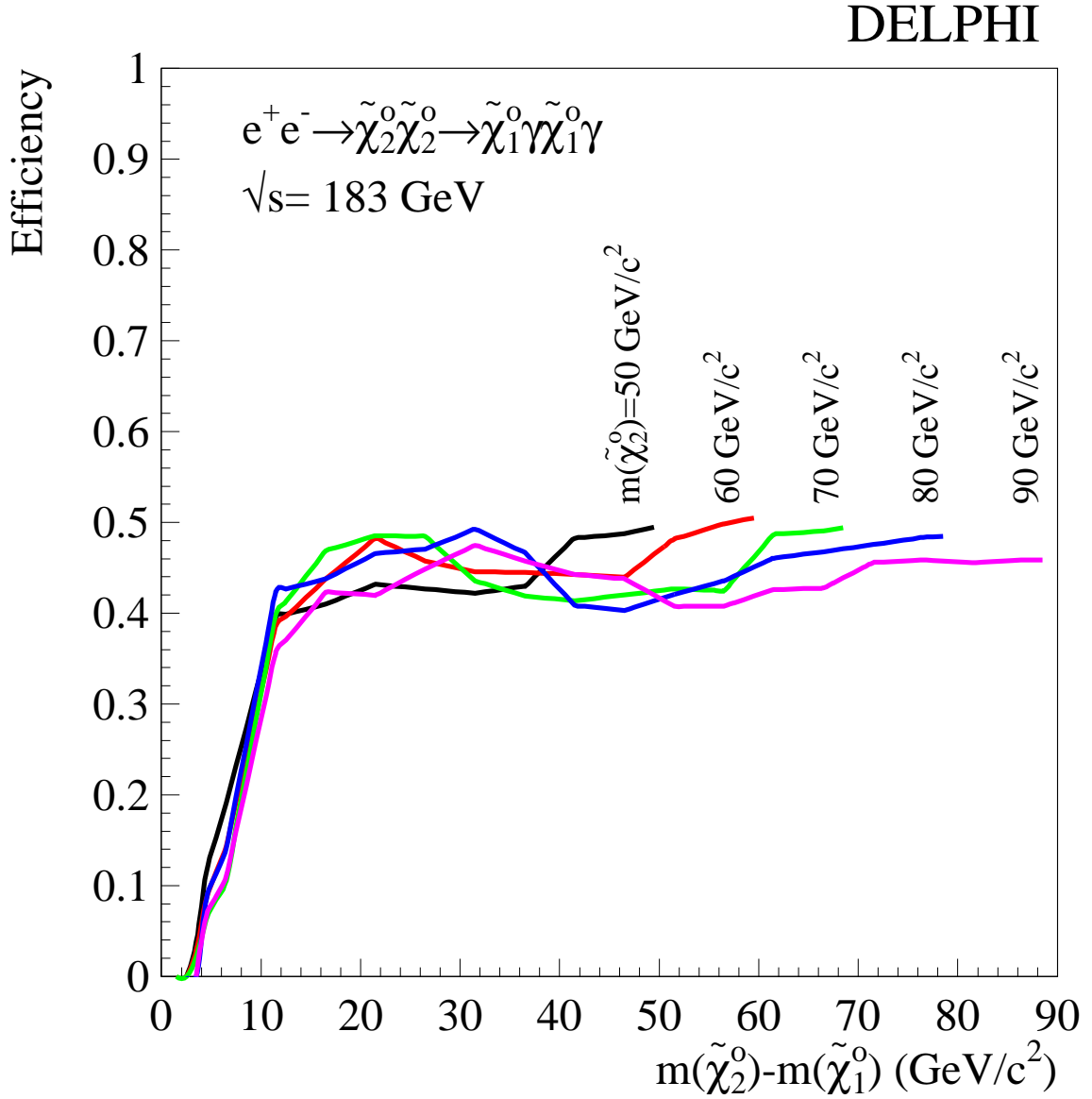


Figure 2: Efficiency at $\sqrt{s} = 183 \text{ GeV}$ for the process $e^+e^- \rightarrow \tilde{\chi}_2^0 \tilde{\chi}_2^0 \rightarrow \tilde{\chi}_1^0 \gamma \tilde{\chi}_1^0 \gamma$ as a function of $m_{\tilde{\chi}_2^0} - m_{\tilde{\chi}_1^0}$ for some given values of $m_{\tilde{\chi}_2^0}$. The efficiencies apply for any generic $e^+e^- \rightarrow YY \rightarrow X\gamma X\gamma$ reaction with the massive X particle remaining undetected. The efficiency includes contributions from the trigger and the selections described in Section 4, including the requirement of kinematic compatibility between the selected events and the signal for each given pair of $Y = \tilde{\chi}_2^0$, $X = \tilde{\chi}_1^0$ masses.

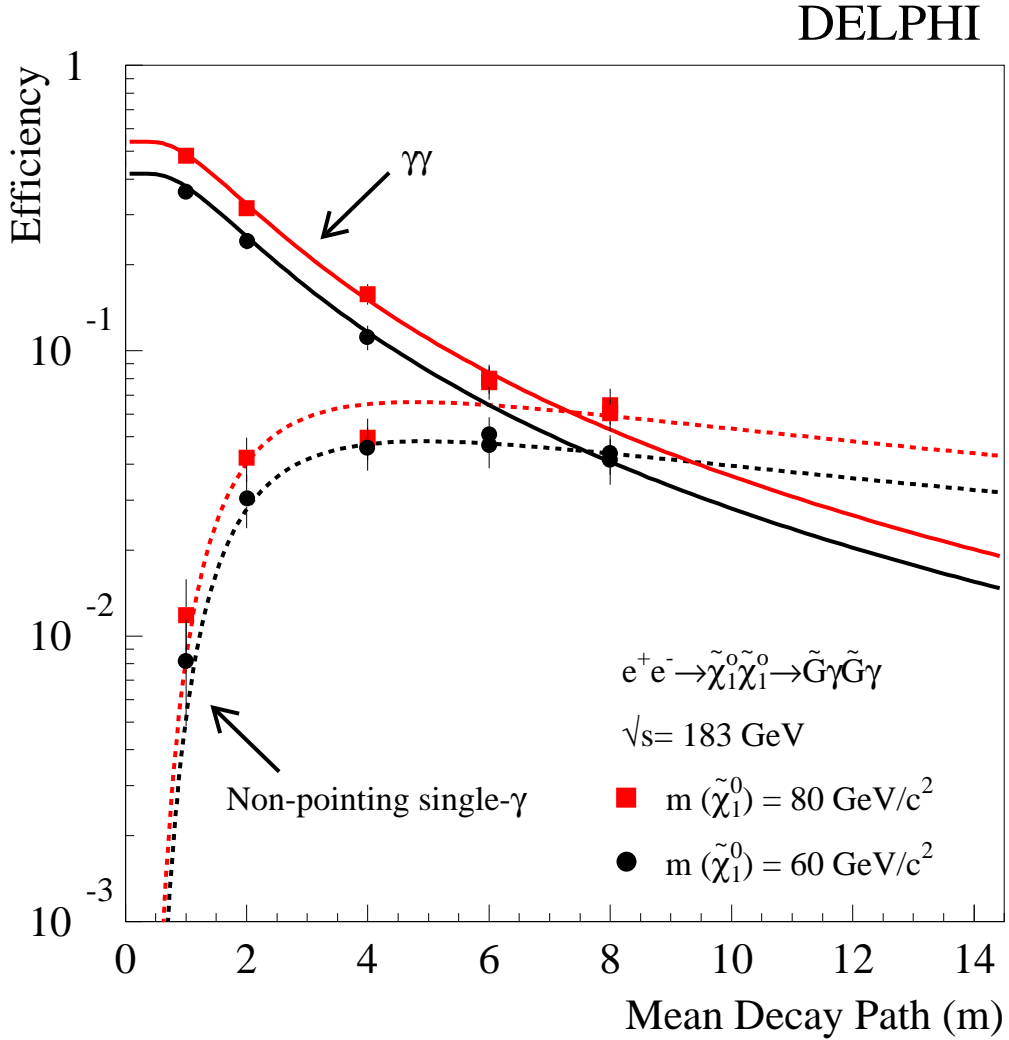


Figure 3: Selection efficiency at $\sqrt{s} = 183 \text{ GeV}$ for the process $e^+e^- \rightarrow \tilde{\chi}_1^0 \tilde{\chi}_1^0 \rightarrow \tilde{G} \gamma \tilde{G} \gamma$ as a function of the neutralino mean decay path for two neutralino masses, namely $m_{\tilde{\chi}_1^0} = 60$ and $80 \text{ GeV}/c^2$. The efficiencies for non-pointing, single photons are compared with the ones of the two-photon search. The curves correspond to a parametrization, while the dots describe the efficiencies obtained with a complete simulation of the DELPHI detector. The trigger efficiency is included.

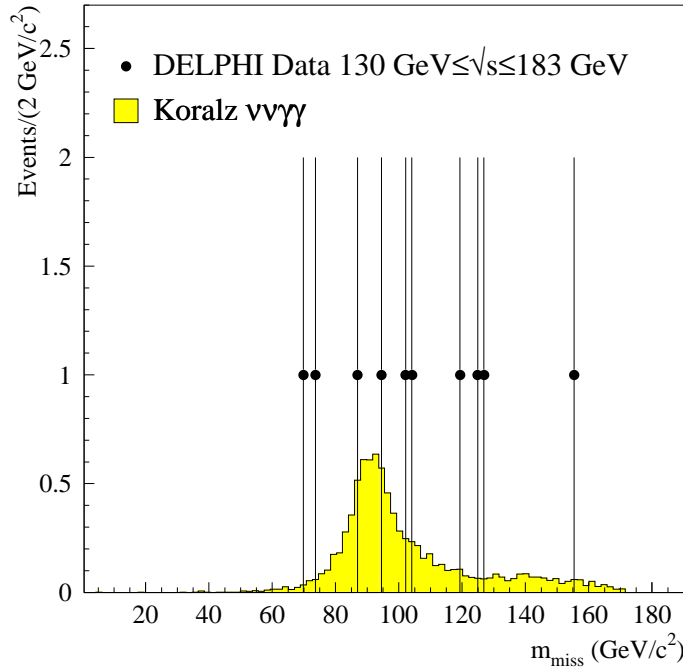


Figure 4: Missing mass distribution of the events passing the preselection, obtained by summing up all the data collected at centre-of-mass energies between 130 and 183 GeV.

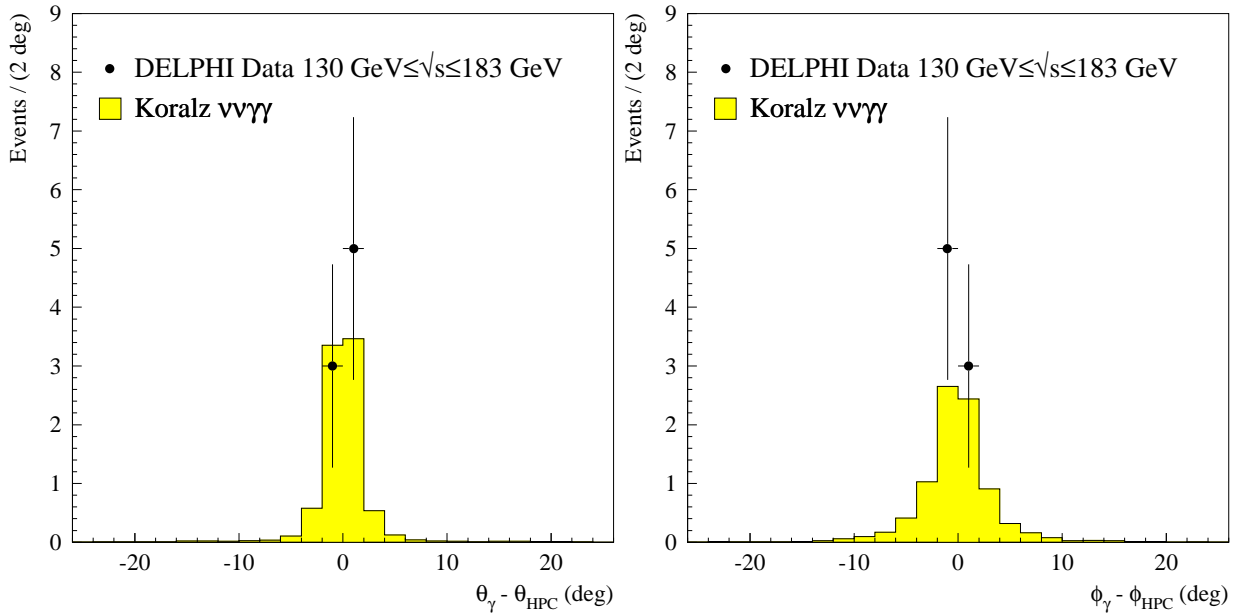


Figure 5: Difference in angle (for the θ and ϕ projections) between the direction of the HPC shower axis and the straight line passing through the photon shower barycentre and the beam interaction region, as observed in all photons detected by the HPC and belonging to the preselected sample of photon-pair events.

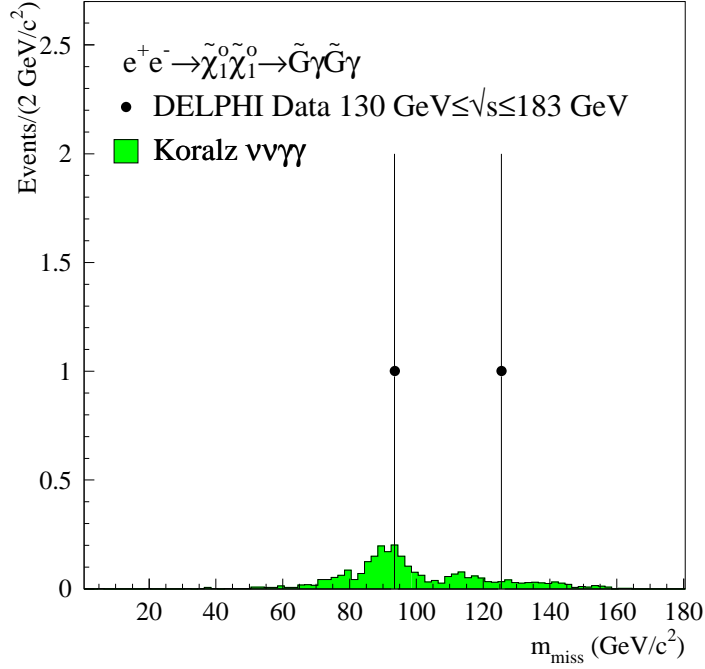


Figure 6: Missing mass distribution of the events passing the final event selection for the case of a massless X particle escaping detection obtained by summing up all the data collected at centre-of-mass energies between 130 and 183 GeV.

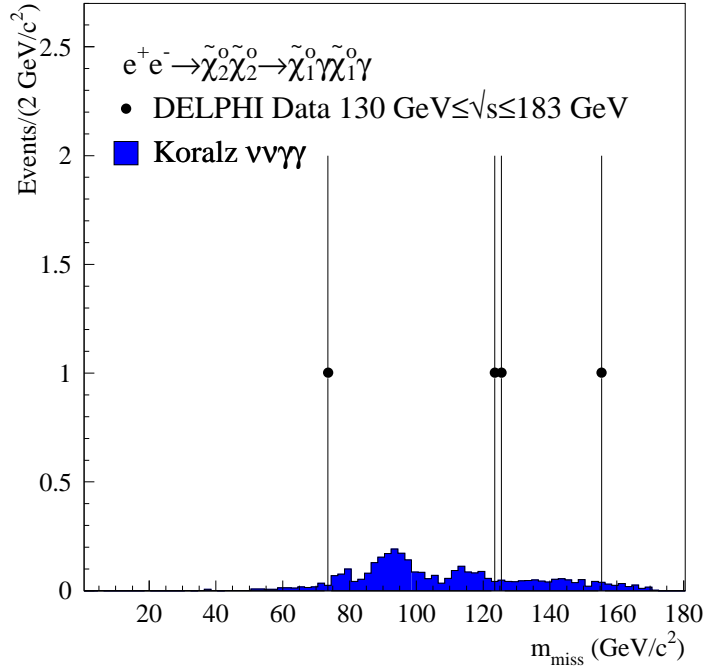


Figure 7: Missing mass distribution of the events passing the final event selection for the case of a massive X particle escaping detection, obtained by summing up all the data collected at centre-of-mass energies between 130 and 183 GeV.

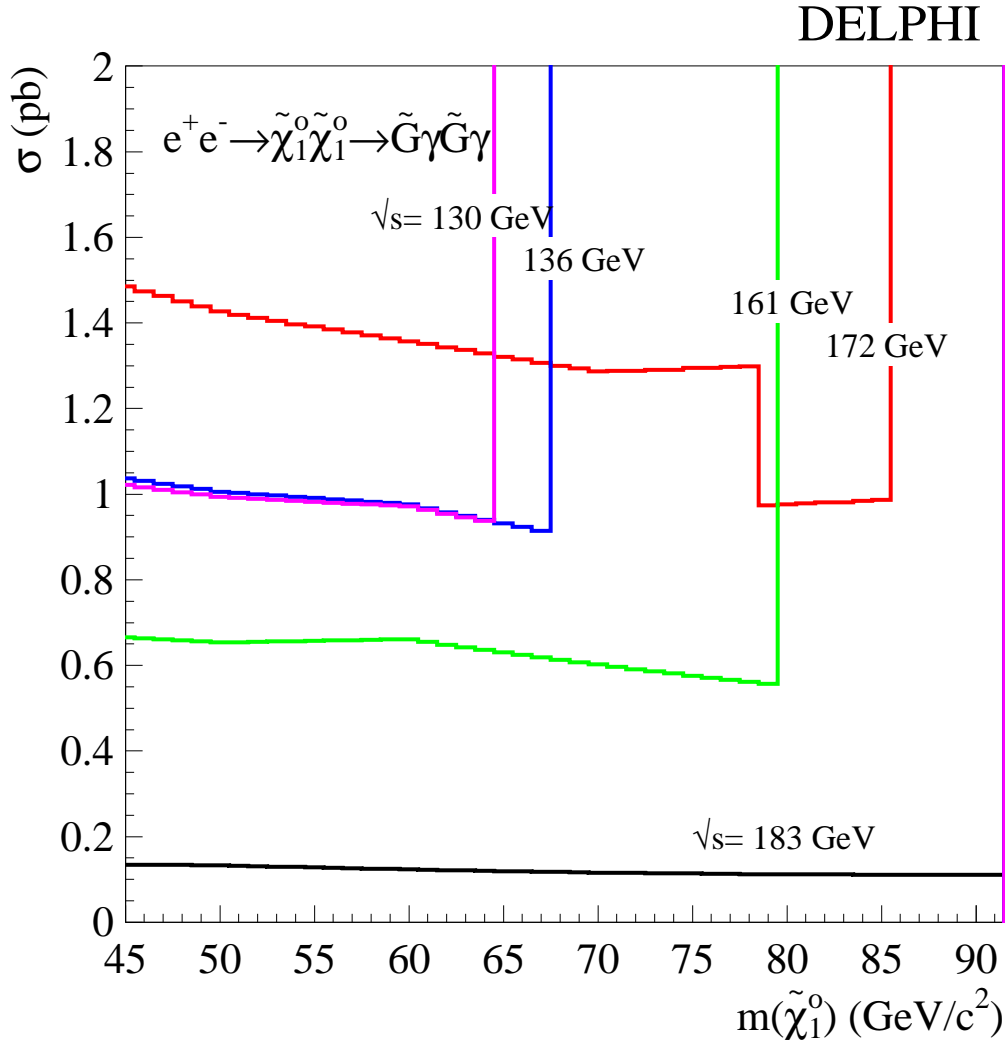


Figure 8: Upper limits at 95% confidence level on the cross-section at the various centre-of-mass energies for the process $e^+e^- \rightarrow \tilde{\chi}_1^0 \tilde{\chi}_1^0 \rightarrow \tilde{G}\gamma\tilde{G}\gamma$ as a function of the $\tilde{\chi}_1^0$ mass assuming $\text{BR}(\tilde{\chi}_1^0 \rightarrow \tilde{G}\gamma)=1$. The limits apply for any generic process of the type $e^+e^- \rightarrow YY \rightarrow X\gamma X\gamma$ where X is a massless undetected particle.

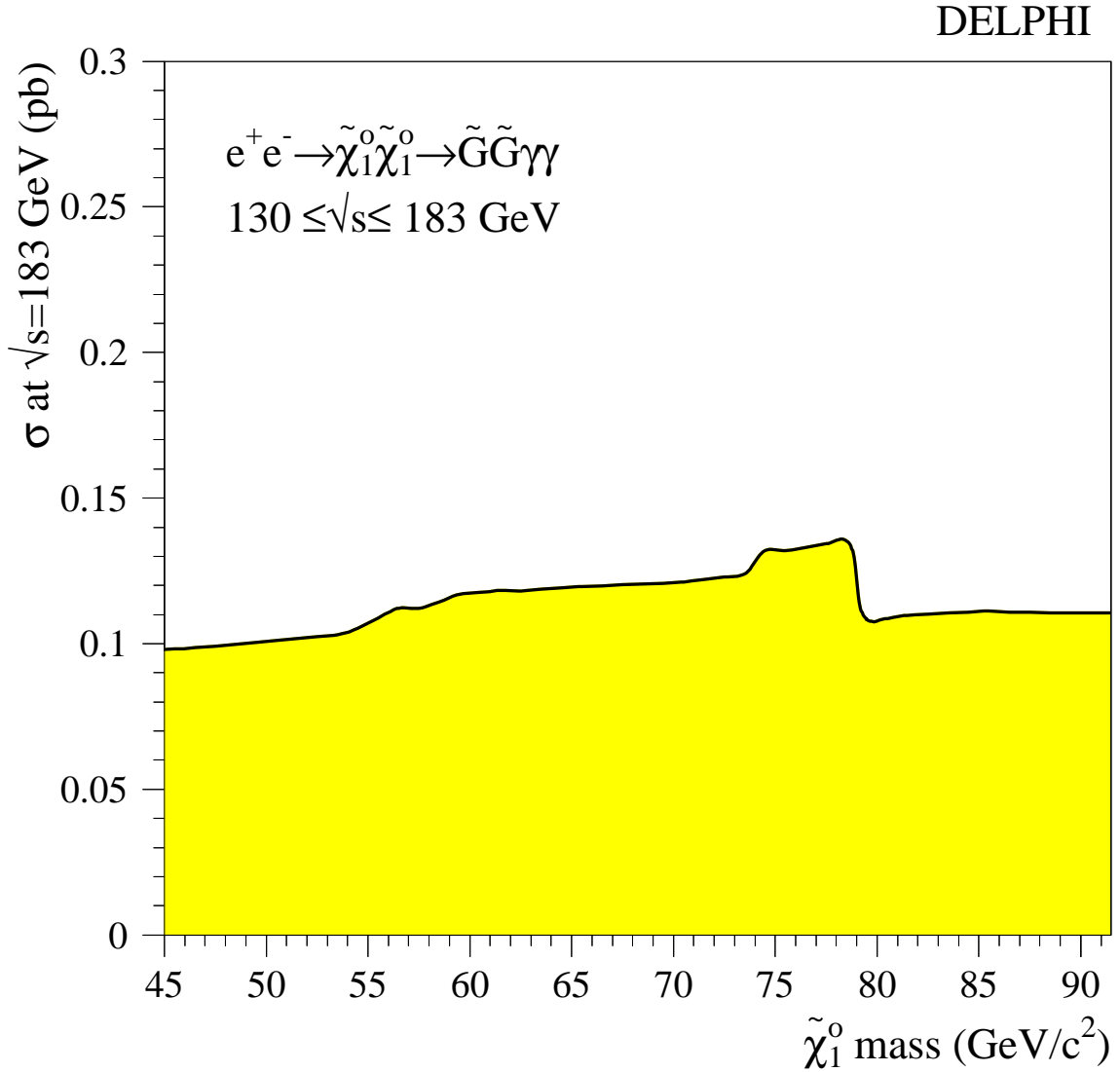


Figure 9: Upper limit at 95% confidence level on the cross-section at $\sqrt{s} = 183$ GeV for the process $e^+e^- \rightarrow \tilde{\chi}_1^0 \tilde{\chi}_1^0 \rightarrow \tilde{G} \tilde{G} \gamma \gamma$ as a function of the $\tilde{\chi}_1^0$ mass assuming $\text{BR}(\tilde{\chi}_1^0 \rightarrow \tilde{G} \gamma) = 1$. The limit applies for any generic process of the type $e^+e^- \rightarrow YY \rightarrow X\gamma X\gamma$ where X is a massless undetected particle. The limit is obtained by combining all the data taken at centre-of-mass energies from 130 GeV to 183 GeV, assuming the signal cross-section to scale as β_Y^3/s .

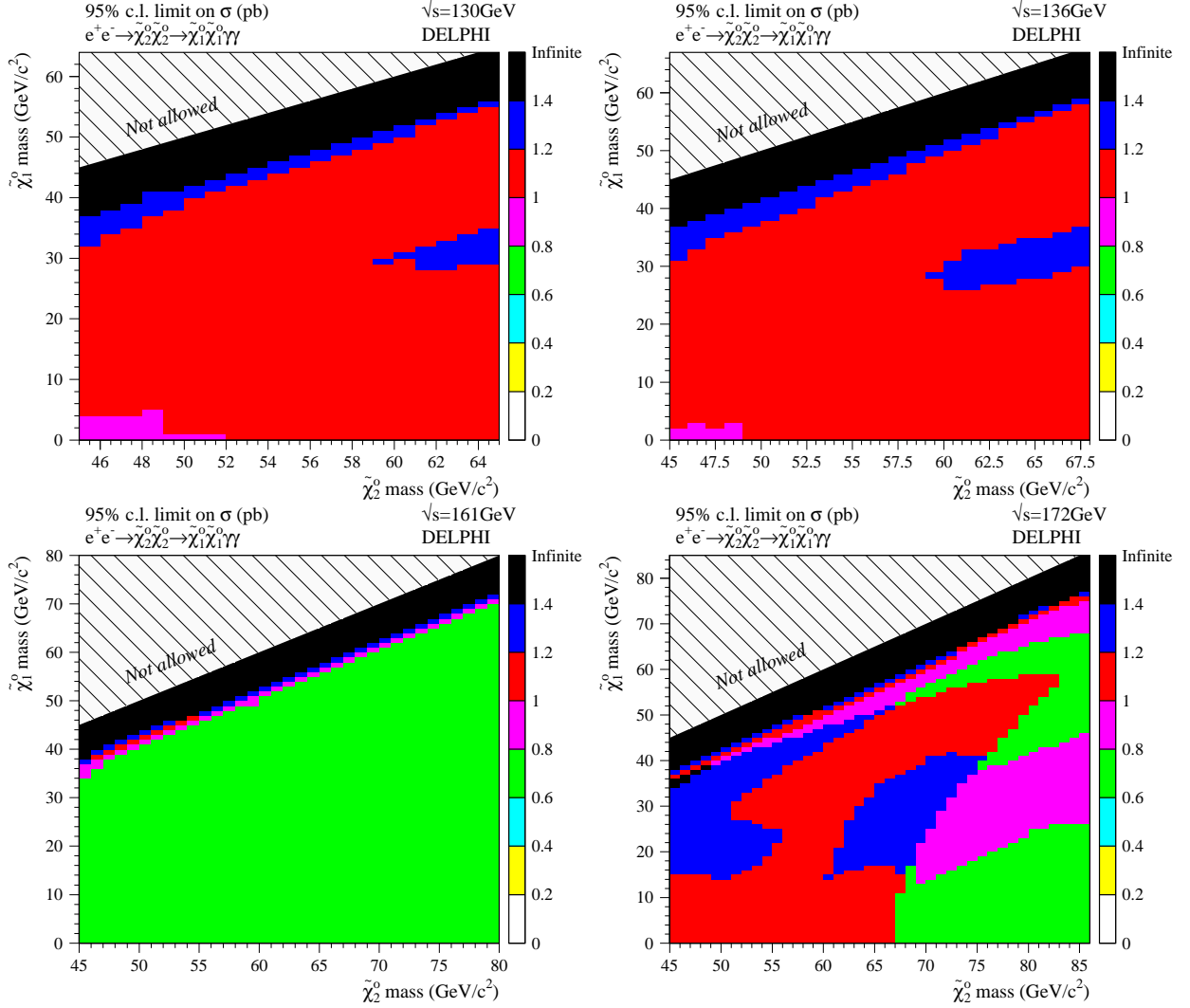


Figure 10: Upper limits at 95% confidence level on the cross-section for the process $e^+e^- \rightarrow \tilde{\chi}_2^0 \tilde{\chi}_2^0 \rightarrow \tilde{\chi}_1^0 \gamma \tilde{\chi}_1^0 \gamma$ as a function of $m_{\tilde{\chi}_2^0}$ and $m_{\tilde{\chi}_1^0}$ at the various centre-of-mass energies: 130 GeV (top left), 136 GeV (top right), 161 GeV (bottom left), 172 GeV (bottom right). A 100% branching ratio is assumed for the decay $\tilde{\chi}_2^0 \rightarrow \tilde{\chi}_1^0 \gamma$. The limits apply for any generic process of the type $e^+e^- \rightarrow YY \rightarrow X\gamma X\gamma$ where X is a massive undetected particle.

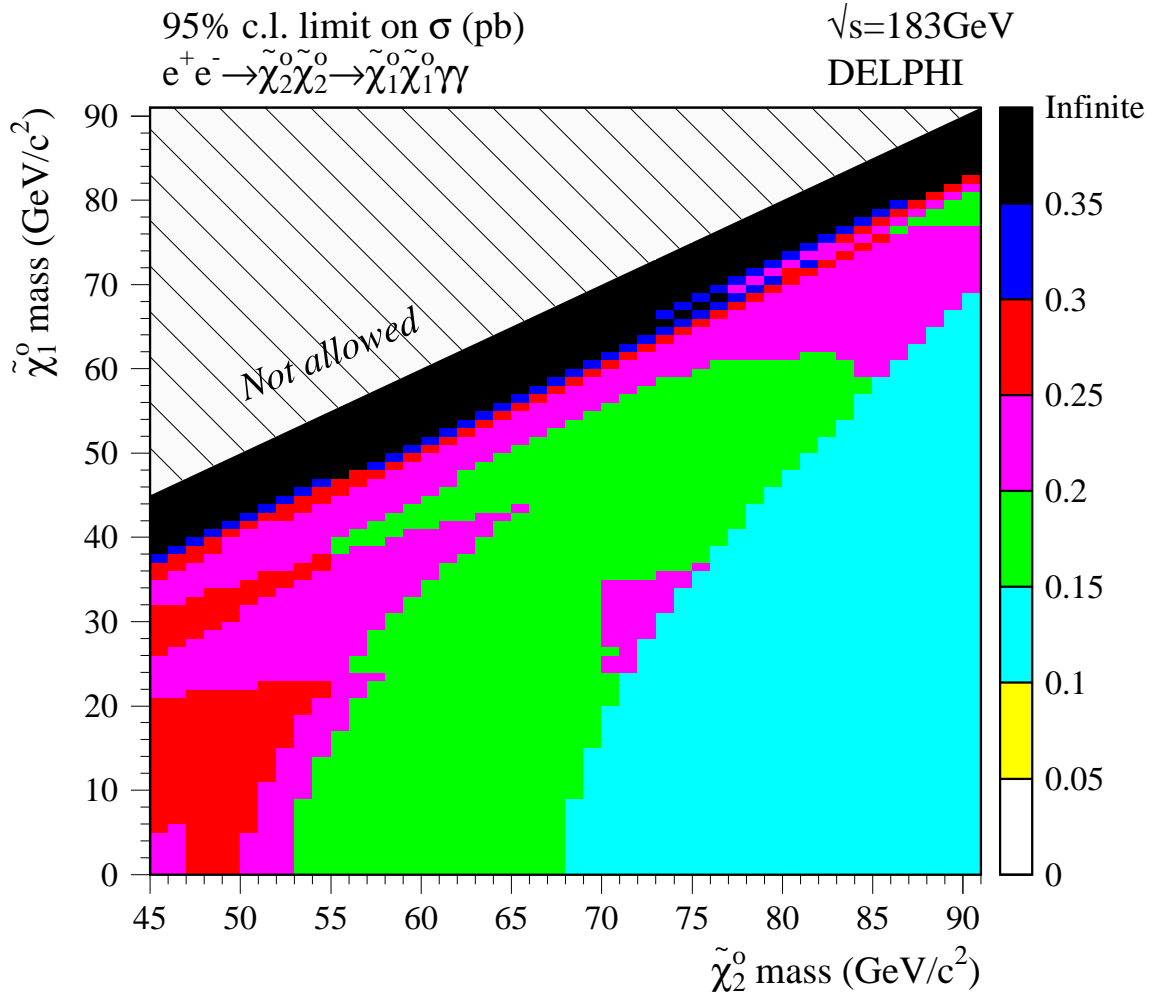


Figure 11: Upper limit at 95% confidence level on the cross-section for the process $e^+e^- \rightarrow \tilde{\chi}_2^0 \tilde{\chi}_2^0 \rightarrow \tilde{\chi}_1^0 \gamma \tilde{\chi}_1^0 \gamma$ as a function of $m_{\tilde{\chi}_2^0}$ and $m_{\tilde{\chi}_1^0}$ at $\sqrt{s} = 183$ GeV. A 100% branching ratio is assumed for the decay $\tilde{\chi}_2^0 \rightarrow \tilde{\chi}_1^0 \gamma$. The limit applies for any generic process of the type $e^+e^- \rightarrow YY \rightarrow X\gamma X\gamma$ where X is a massive undetected particle.

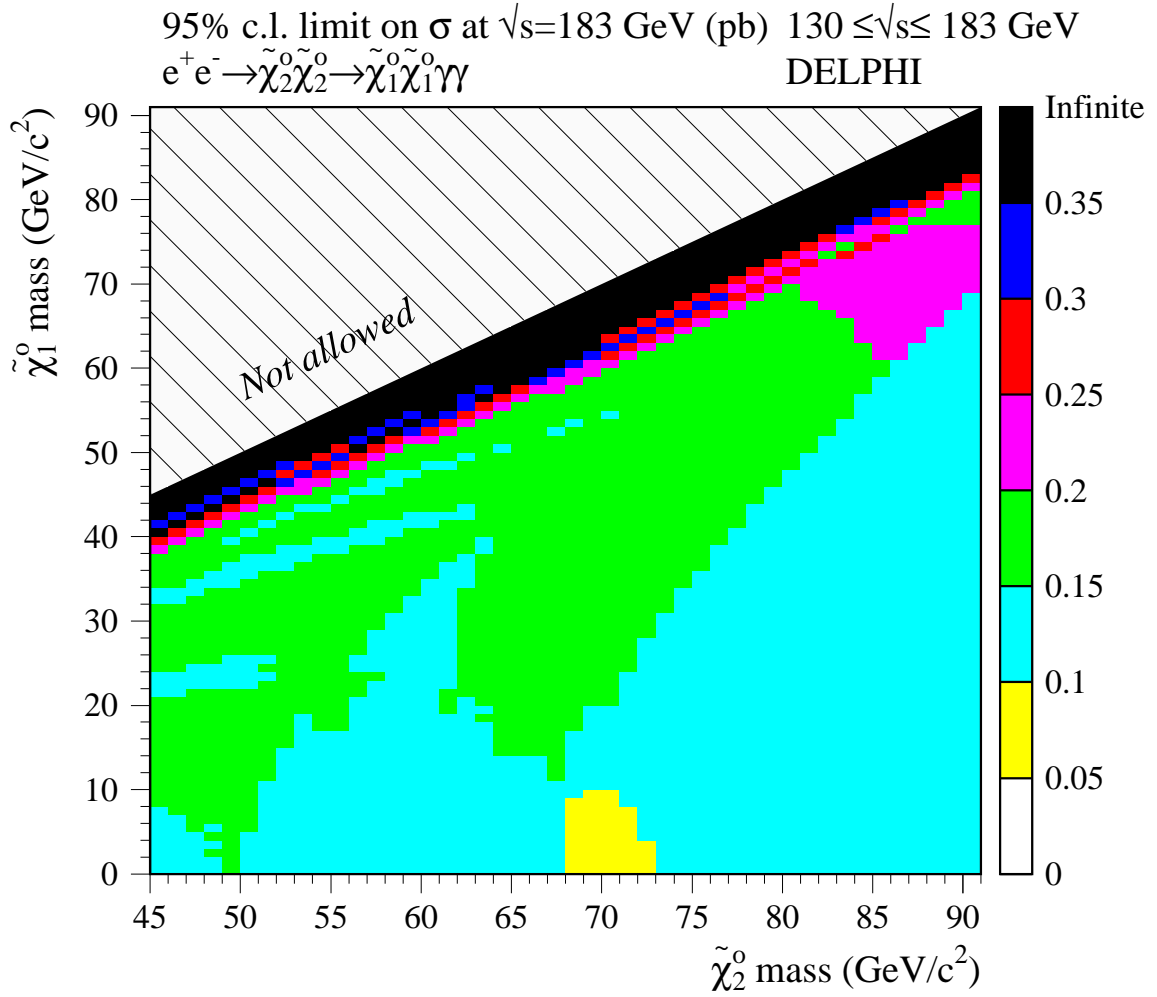


Figure 12: Upper limit at 95% confidence level on the cross-section at $\sqrt{s} = 183$ GeV for the process $e^+e^- \rightarrow \tilde{\chi}_2^0 \tilde{\chi}_2^0 \rightarrow \tilde{\chi}_1^0 \gamma \tilde{\chi}_1^0 \gamma$ as a function of $m_{\tilde{\chi}_2^0}$ and $m_{\tilde{\chi}_1^0}$ as obtained by combining all data taken in the range $130 \text{ GeV} \leq \sqrt{s} \leq 183 \text{ GeV}$. A 100% branching ratio is assumed for the decay $\tilde{\chi}_2^0 \rightarrow \tilde{\chi}_1^0 \gamma$. The limit applies for any generic process of the type $e^+e^- \rightarrow YY \rightarrow X\gamma X\gamma$ where X is a massive undetected particle. The signal cross-section is assumed to scale as β_Y^3/s .

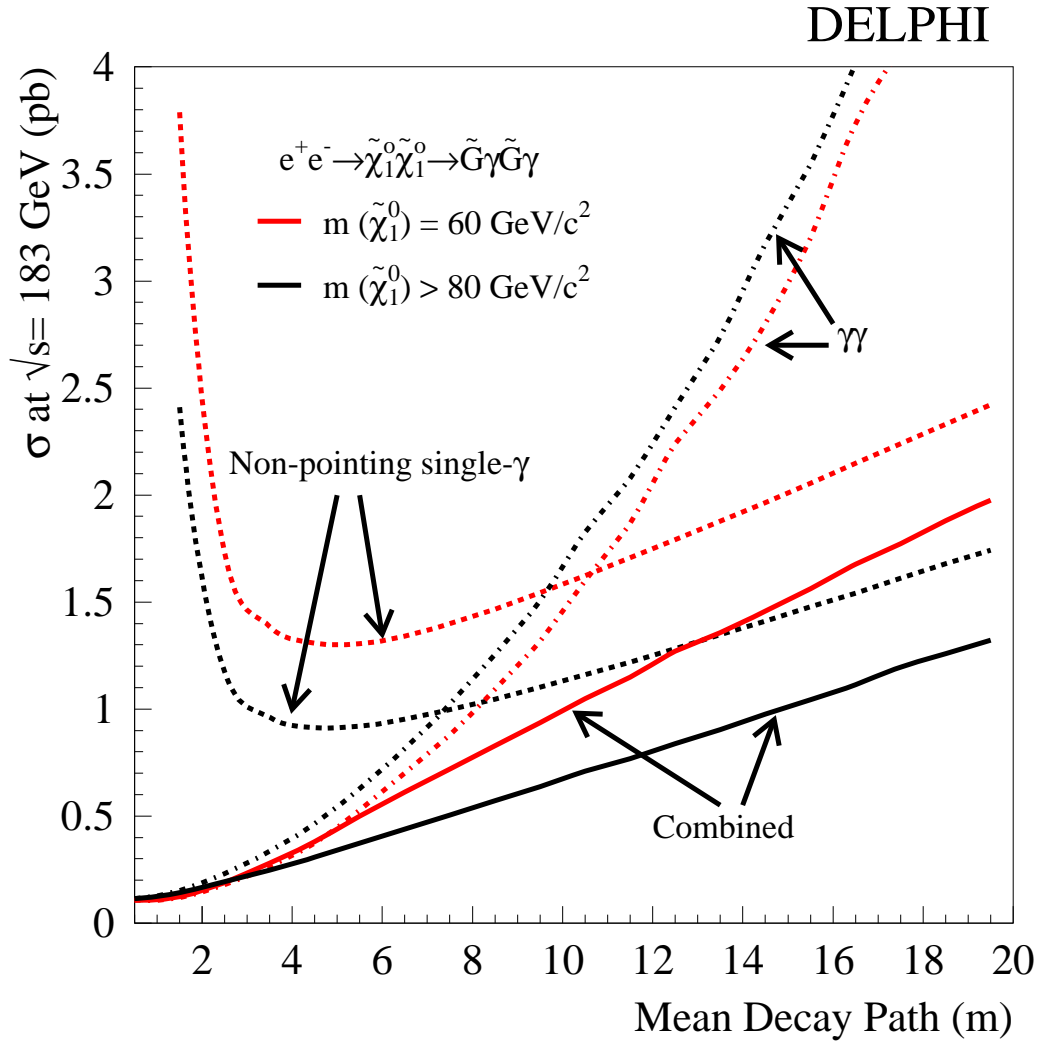


Figure 13: Upper limits at the 95% confidence level on the cross-section at $\sqrt{s} = 183 \text{ GeV}$ for the process $e^+e^- \rightarrow \tilde{\chi}_1^0 \tilde{\chi}_1^0 \rightarrow \tilde{G} \gamma \tilde{G} \gamma$ as a function of the neutralino mean decay path for two hypotheses on the neutralino mass: $m_{\tilde{\chi}_1^0} = 60 \text{ GeV}/c^2$ and $80 < m_{\tilde{\chi}_1^0} < 91 \text{ GeV}/c^2$. A 100% branching ratio is assumed for the decay $\tilde{\chi}_1^0 \rightarrow \tilde{G} \gamma$. The limit is obtained by combining the data collected at \sqrt{s} from 130 to 183 GeV. The different curves correspond to the results obtained from the analysis of acoplanar two-photon events, from the search for single non-pointing photons and from the combination of the two analyses.

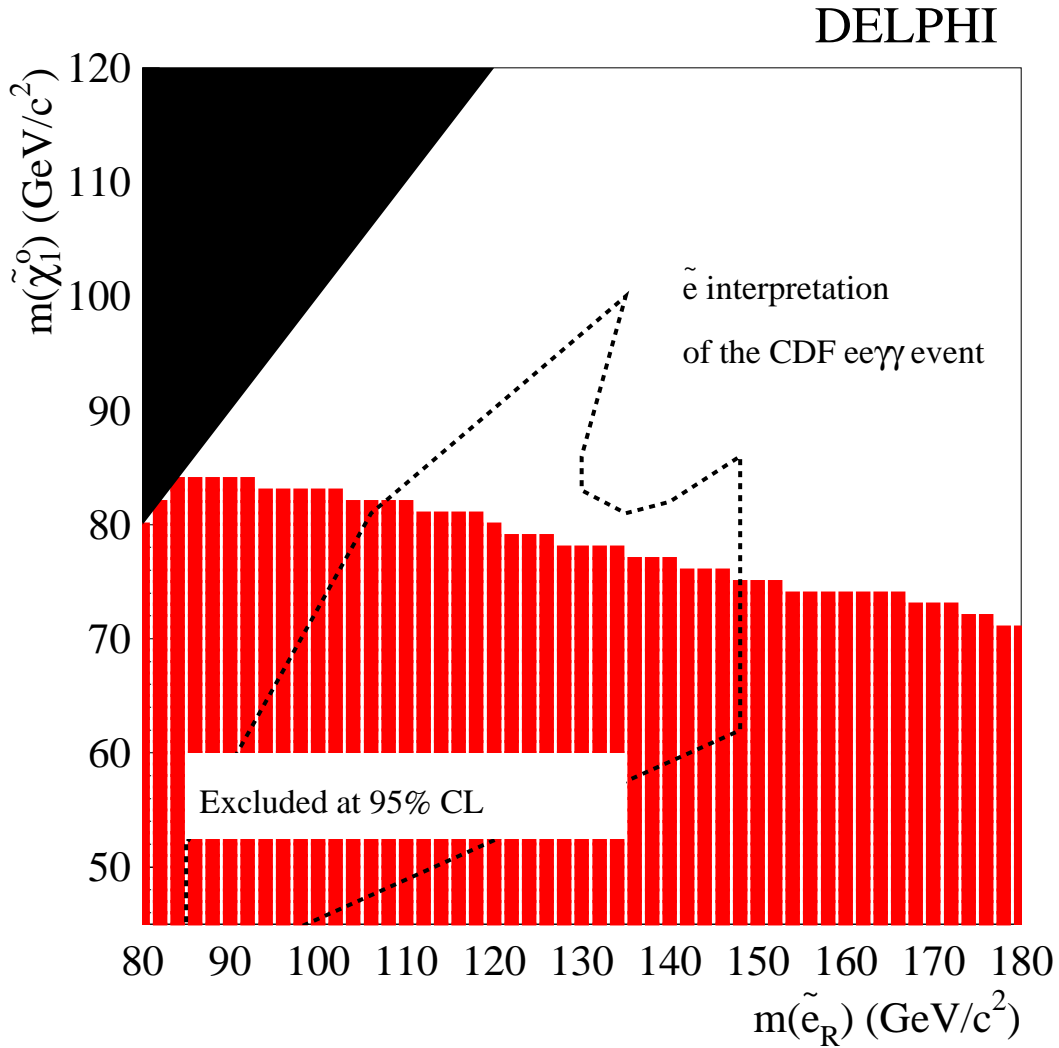


Figure 14: The region excluded by DELPHI data in the $m_{\tilde{\chi}_1^0}$ versus $m_{\tilde{e}_R}$ plane as compared to the region inside the dotted line which is compatible with the selectron interpretation of the CDF $ee\gamma\gamma$ event when a 100% branching ratio is assumed for the decay $\tilde{\chi}_1^0 \rightarrow \tilde{G}\gamma$.

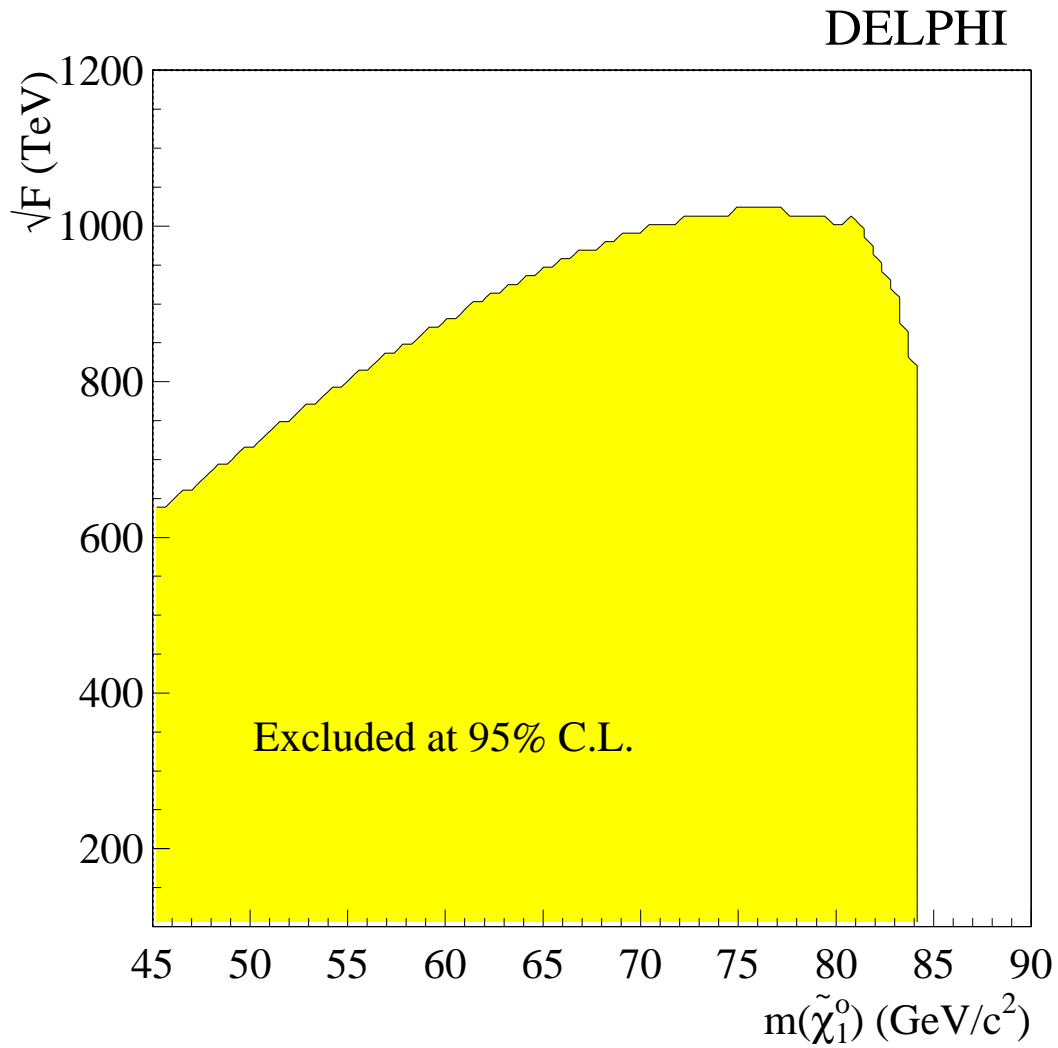


Figure 15: Lower bound on the SUSY breaking scale \sqrt{F} as a function of the neutralino mass $m_{\tilde{\chi}_1^0}$ in the hypothesis that $\tilde{\chi}_1^0$ is pure Bino and $m_{\tilde{e}_R} = 1.1 m_{\tilde{\chi}_1^0}$.